nature neuroscience

ARTICLES

https://doi.org/10.1038/s41593-020-0617-7

Orexin signaling in GABAergic lateral habenula neurons modulates aggressive behavior in male mice

Meghan E. Flanigan[1,2], Hossein Aleyasin[1,2], Long Li[1,2], C. Joseph Burnett[1,2], Kenny L. Chan[1,2], Katherine B. LeClair[1,2], Elizabeth K. Lucas[1,2,3], Bridget Matikainen-Ankney[1,2], Romain Durand-de Cuttoli[1,2], Aki Takahashi[1,2,4], Caroline Menard[1,2,5], Madeline L. Pfau[1,2], Sam A. Golden[6], Sylvain Bouchard[1,2], Erin S. Calipari[1,2,7], Eric J. Nestler[1,2], Ralph J. DiLeone[8], Akihiro Yamanaka[9], George W. Huntley[1,2], Roger L. Clem[1,2] and Scott J. Russo[1,2] ✉

Heightened aggression is characteristic of multiple neuropsychiatric disorders and can have various negative effects on patients, their families and the public. Recent studies in humans and animals have implicated brain reward circuits in aggression and suggest that, in subsets of aggressive individuals, domination of subordinate social targets is reinforcing. In this study, we showed that, in male mice, orexin neurons in the lateral hypothalamus activated a small population of glutamic acid decarboxylase 2 (GAD2)-expressing neurons in the lateral habenula (LHb) via orexin receptor 2 (OxR2) and that activation of these GAD2 neurons promoted male–male aggression and conditioned place preference for aggression-paired contexts. Moreover, LHb GAD2 neurons were inhibitory within the LHb and dampened the activity of the LHb as a whole. These results suggest that the orexin system is important for the regulation of inter-male aggressive behavior and provide the first functional evidence of a local inhibitory circuit within the LHb.

Various psychiatric syndromes are associated with increased risk for pathological aggressive behaviors, including autism spectrum disorders[1], attention-deficit hyperactivity disorder[2], personality disorders[3] and mood disorders[4]. It has been hypothesized that brain reward systems controlling the valence of social interactions might be dysregulated in these disorders, leading to heightened aggression that is reinforcing[5–7]. Recent studies in animals found that a subset of highly aggressive male mice will lever press for access to subordinate intruders[8] and form conditioned place preferences (CPPs) for contexts that are associated with access to subordinate intruders[9]. This suggests that male mice find the domination of subordinate social targets to be rewarding and display high motivation for repeated opportunities to fight.

Considering the strong motivational component to aggressive behavior, there has been increasing interest in the role that reward circuitry plays in controlling aggression. One region in particular, the LHb, has been newly identified as a potential modulator of the valence of aggressive social interactions[10]. The LHb is a critical node within the reward circuitry of humans and nonhuman animals that, when activated, promotes negative emotional states predominantly through indirect inhibition of midbrain dopamine neurons[11,12]. LHb function is disrupted in various neuropsychiatric disorders associated with aggression, including mood disorders[13,14]. In zebrafish and mice, functional manipulation of LHb neurons alters aggression, its rewarding properties and the likelihood of 'winning' a fight. Specifically, optogenetic inhibition of mouse LHb neurons during the test phase of the aggression CPP task increases the time spent in the aggression-paired context, whereas optogenetic activation of these neurons reduces it[9]. In addition, direct optogenetic activation of a zebrafish homologue of the mammalian LHb results in increased probability of losing a fight[15]. Although these results highlight the importance of the LHb in aggression, the specific LHb inputs as well as the local LHb circuitry regulating aggression remain largely unknown.

Previous studies described the LHb as consisting almost exclusively of glutamate projection neurons expressing vesicular glutamate transporter 2 (vGlut2)[16]. However, there is recent histologic and single-cell sequencing evidence that the LHb contains a small population of cells that express GAD2 (refs. [17,18]), which is a general marker of GABAergic inhibitory neurons. Despite these studies, very little is known about GAD2 neurons in the LHb, including which inputs target them or whether they are capable of providing local inhibition, long-range inhibition or both. However, it has been reported that they are enriched in receptors for several hypothalamic-derived neuropeptides and hormones, including OxR2 (refs. [17,18]). As orexin neuron cell bodies are located solely in the lateral hypothalamus (LH)[19], this suggests that LHb GAD2 neurons are modulated by projections from lateral hypothalamic orexin

[1]Nash Family Department of Neuroscience, Icahn School of Medicine at Mount Sinai, New York, NY, USA. [2]Friedman Brain Institute, Icahn School of Medicine at Mount Sinai, New York, NY, USA. [3]Department of Molecular Biomedical Sciences, North Carolina State University, Raleigh, NC, USA. [4]Laboratory of Behavioral Neuroendocrinology, University of Tsukuba, Tsukuba, Ibaraki, Japan. [5]Department of Psychiatry and Neuroscience, Faculty of Medicine and CERVO Brain Research Center, Université Laval, Ville de Québec, QC, Canada. [6]Department of Biological Structure, University of Washington, Seattle, WA, USA. [7]Department of Pharmacology, Vanderbilt University School of Medicine, Nashville, TN, USA. [8]Department of Psychiatry, Yale University, New Haven, CT, USA. [9]Department of Neuroscience II, Research Institute of Environmental Medicine, Nagoya University, Nagoya, Japan. ✉e-mail: scott.russo@mssm.edu

neurons. Although not previously implicated in aggression, orexin has been strongly implicated in arousal[20], social behavior[21] and a wide array of motivated behaviors[22–26].

In this study, we sought to characterize the cell-type-specific dynamics of LHb neurons during aggression and to determine whether orexin release onto GAD2 LHb neurons influences aggressive behavior. First, we showed that LHb vGlut2 neurons reduced their activity during aggression, whereas GAD2 LHb neurons increased their activity. Next, we found that GAD2 LHb neurons exerted local inhibitory control over the LHb as a whole and that direct optogenetic manipulation of GAD2 LHb neurons altered aggression and aggression CPP. Further, we demonstrated that direct optogenetic modulation of orexin inputs from the lateral hypothalamus (LH) to the LHb promoted aggression and aggression CPP through an OxR2-dependent mechanism. Our findings indicate that cell-type-specific engagement of orexin signaling in the LHb is important for modulating aggression, and they extend orexin's known role in motivation to the social realm.

Results

Aggression is associated with reduced total LHb activity. To first investigate patterns of total LHb activity associated with repeated aggressive social encounters, we injected nonconditional AAV-GCaMP6 into the LHb, implanted a fiber above the cells and measured fluorescent calcium transients in highly aggressive (AGG) and non-aggressive (NON) CD-1 wild-type mice during the resident intruder (RI) and aggression CPP tests using fiber photometry (Fig. 1a,b). In the RI test, male CD-1 outbred mice were exposed to submissive male C57BL/6J intruders for 5 min in their home cage and allowed to freely interact. CD-1 mice displayed individual variation in aggressive behaviors in this task, with some animals consistently fighting with low attack latencies (termed aggressors, AGGs) and some animals never engaging in any aggressive behaviors (termed non-aggressors, NONs). Notably, because CD-1 resident mice are vastly larger and more dominant than C57BL/6J intruder mice, AGGs engaging in fighting during RI consistently subordinate intruder mice and are never themselves attacked by the intruder. In aggression CPP, animals were conditioned in two 10-min sessions per day for 3 d to associate distinct contexts with the presence or absence of subordinate intruders. On the test day, experimental mice were given free access to both contexts (in the absence of intruders), and the time spent in each context was measured to determine the valence of the social encounter. NONs formed an aversion for the intruder-paired context, whereas AGGs formed a preference for it, suggesting that AGGs find these social encounters rewarding and will seek out opportunities for aggression[9].

Considering that optogenetic inhibition of the LHb has been shown to promote aggression and aggression CPP[9], we hypothesized that aggressive behaviors would be associated with reductions in LHb activity. Consistent with our hypothesis, AGGs displayed reductions in LHb activity upon biting an intruder (Fig. 1d,e). Conversely, NONs displayed increases in LHb activity upon intruder approaches (Fig. 1f,g). AGGs and NONs also displayed opposing LHb responses to withdrawals from social bouts, with AGGs showing increases in LHb activity upon withdrawals from aggressive social bouts and NONs showing decreases in LHb activity upon withdrawals from non-aggressive social bouts (Fig. 1h–k). Notably, these LHb responses to social targets during RI in AGGs were observed on both day 1 of RI (Extended Data Fig. 1) and day 3 of RI (Fig. 1d–j). Over the 3 d of RI, AGGs increased their aggression toward the intruder, attacking with shorter latencies on day 3 than on day 1 (Fig. 1c). This is consistent with previous studies describing a phenomenon called 'the winner effect,' whereby prior winning experience increases aggression toward future social targets[27]. Notably, the observed increase in aggression on day 3 of RI was associated with decreased LHb activity across the RI session compared to day 1 of RI (Fig. 1l–m). However, NONs trended only toward increased LHb activity across the RI session on day 3 compared to day 1 ($P=0.08$; Fig. 1n,o).

To determine whether the LHb is capable of encoding contextual information about the rewarding properties of aggressive social encounters, we next performed fiber photometry in AGGs and NONs during the test phase of aggression CPP. We found that AGGs displayed reduced LHb activity in the paired context of the CPP chamber compared to the unpaired context (Fig. 1p,q). Similarly, NONs showed a trend toward increased LHb activity in the paired context of the CPP chamber compared to the unpaired context ($P=0.10$; Fig. 1r,s). In addition, CPP scores of AGGs and NONs were negatively correlated with LHb activity in the paired context (Extended Data Fig. 1). Together, these data indicate that the LHb is

Fig. 1 | Aggressive behaviors are associated with decreased LHb activity. a, Surgical manipulations and representative viral infection for LHb photometry experiments (scale bar, 400 µm). **b**, Experimental timeline for LHb photometry experiments. **c**, AGGs displayed reduced attack latency on day 3 compared to day 1 of RI (one-way repeated-measures ANOVA, $n=5$ AGGs, $F_{2,8}=74.832$, main effect of day $P=0.04832$; Dunnett's multiple-comparisons test day 1 versus day 3, adjusted $P=0.0327$). **d**, Peri-event plot of AGG LHb activity before and after a bite on day 3 of RI. For all peri-event plots, the black line denotes the mean signals for all animals, whereas the blue shaded region denotes the s.e.m., $n=5$ biologically independent mice, 3–5 bites per mouse. **e**, AGGs displayed a reduction in average LHb activity after a bite (two-tailed paired *t*-test, $n=5$ biologically independent mice, 3–5 bites per mouse, $t_4=4.593$, $P=0.0101$). **f**, Peri-event plot of NON LHb activity before and after an intruder approach on day 3 of RI. The black line denotes the mean signals for all animals, whereas the blue shaded region denotes the s.e.m., $n=5$ biologically independent mice, 3–5 approaches per mouse. **g**, NONs displayed an increase in average LHb activity after an approach (two-tailed paired *t*-test, $n=5$ biologically independent mice, 3–5 approaches per mouse, $t_4=3.450$, $P=0.0261$). **h**, Peri-event plot of AGG LHb activity before and after a withdrawal from an aggressive bout. The black line denotes the mean signals for all animals, whereas the blue shaded region denotes the s.e.m., $n=5$ biologically independent mice, 3–5 withdrawals per mouse. **i**, AGGs displayed an increase in average LHb activity after a withdrawal (two-tailed paired *t*-test, $n=5$ biologically independent mice, 3–5 withdrawals per mouse, $t_4=3.911$, $P=0.0174$). **j**, Peri-event plot of NON LHb activity before and after a withdrawal from a non-aggressive social interaction. The black line denotes the mean signals for all animals, whereas the blue shaded region denotes the s.e.m., $n=5$ biologically independent mice, 3–5 withdrawals per mouse. **k**, NONs displayed a decrease in LHb activity after a withdrawal from a non-aggressive social interaction (two-tailed paired *t*-test, $n=5$ biologically independent mice, 3–5 withdrawals per mouse, $t_4=2.838$, $P=0.0470$). **l**, Representative traces of AGG LHb activity in the absence and presence of an intruder mouse on day 3 of RI. **m**, AGGs displayed reduced LHb activity across 3 d of RI (one-way repeated-measures ANOVA, $n=5$ biologically independent mice, $F_{2,8}=6.294$, $P=0.0228$; Dunnett's test for multiple comparisons, day 1 versus day 3, adjusted $P=0.0228$). **n**, Representative traces of NON LHb activity in the absence and presence of an intruder mouse on day 3 of RI. **o**, NONs displayed a trend toward increased LHb activity across 3 d of RI (one-way repeated-measures ANOVA, $n=5$ mice, $F_{2,14}=3.985$, $P=0.0630$). **p**, Representative trace of AGG LHb activity during the aggression CPP test. **q**, AGGs displayed reduced LHb activity in the paired context compared to the unpaired context during the aggression CPP test (two-tailed paired *t*-test, $n=4$ mice, $t_3=4.080$, $P=0.0266$). **r**, Representative trace of NON LHb activity during the aggression CPP test. **s**, NONs displayed no differences in LHb activity in the paired context compared to the unpaired context during the aggression CPP test (paired *t*-test, $n=4$ mice, $t_3=2.352$, $P=0.1001$). $^*P<0.05$. All data are expressed as mean ± s.e.m.

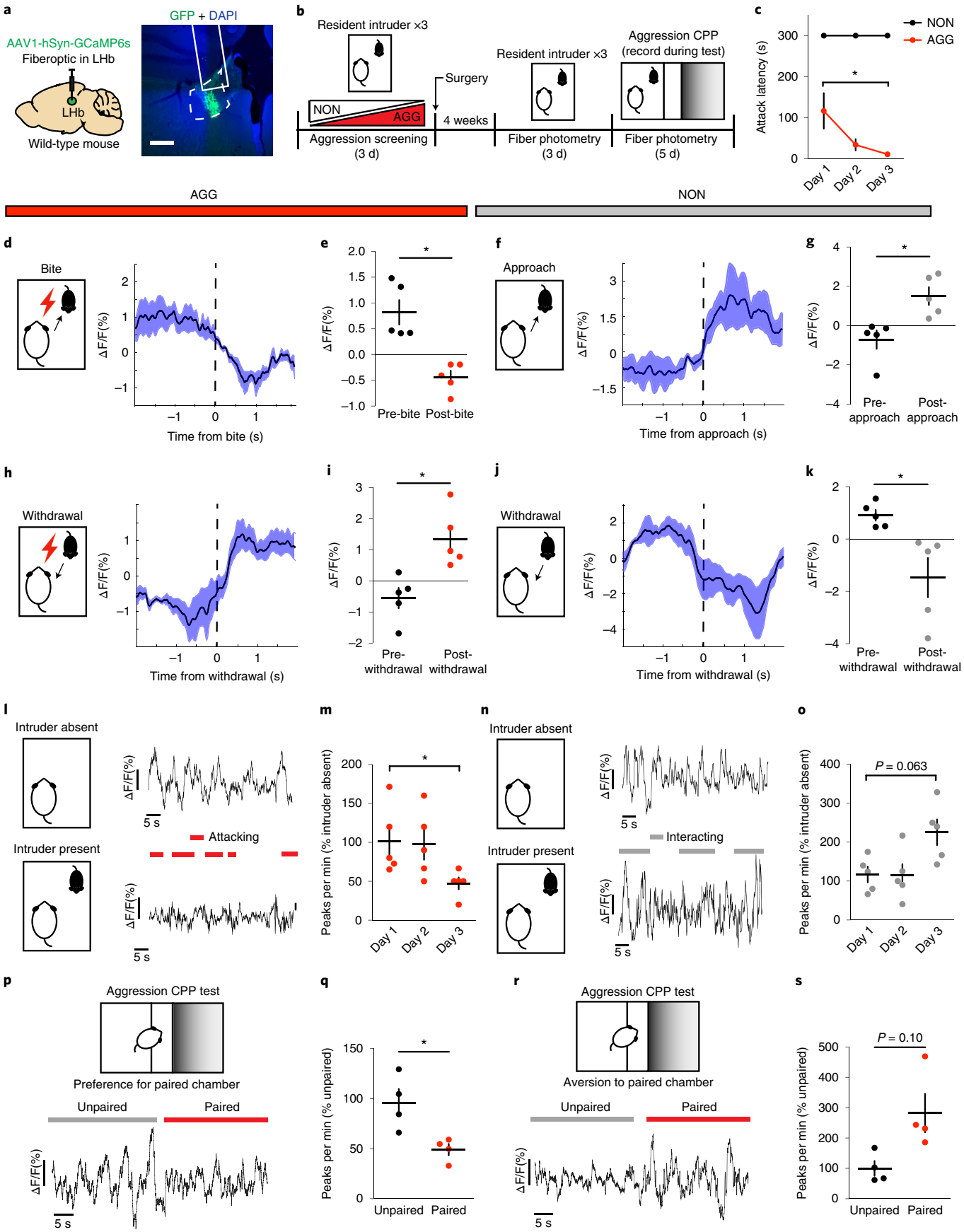
a
GFP + DAPI
AAV1-hSyn-GCaMP6s
Fiberoptic in LHb
LHb
Wild-type mouse
b
Resident intruder ×3
NON
AGG
Surgery
4 weeks
Aggression screening
(3 d)
Resident intruder ×3
Fiber photometry
(3 d)
Aggression CPP
(record during test)
Fiber photometry
(5 d)
c
Attack latency (s)
NON
AGG
Day 1
Day 2
Day 3
AGG
NON
d
Bite
ΔF/F(%)
Time from bite (s)
e
Pre-bite
Post-bite
f
Approach
Time from approach (s)
g
Pre-approach
Post-approach
h
Withdrawal
Time from withdrawal (s)
i
Pre-withdrawal
Post-withdrawal
j
Withdrawal
Time from withdrawal (s)
k
Pre-withdrawal
Post-withdrawal
l
Intruder absent
Intruder present
Attacking
5 s
m
Peaks per min (% intruder absent)
Day 1
Day 2
Day 3
n
Intruder absent
Intruder present
Interacting
5 s
o
P = 0.063
Peaks per min (% intruder absent)
p
Aggression CPP test
Preference for paired chamber
Unpaired
Paired
5 s
q
Peaks per min (% unpaired)
Unpaired
Paired
r
Aggression CPP test
Aversion to paired chamber
Unpaired
Paired
5 s
s
P = 0.10
Peaks per min (% unpaired)
Unpaired
Paired

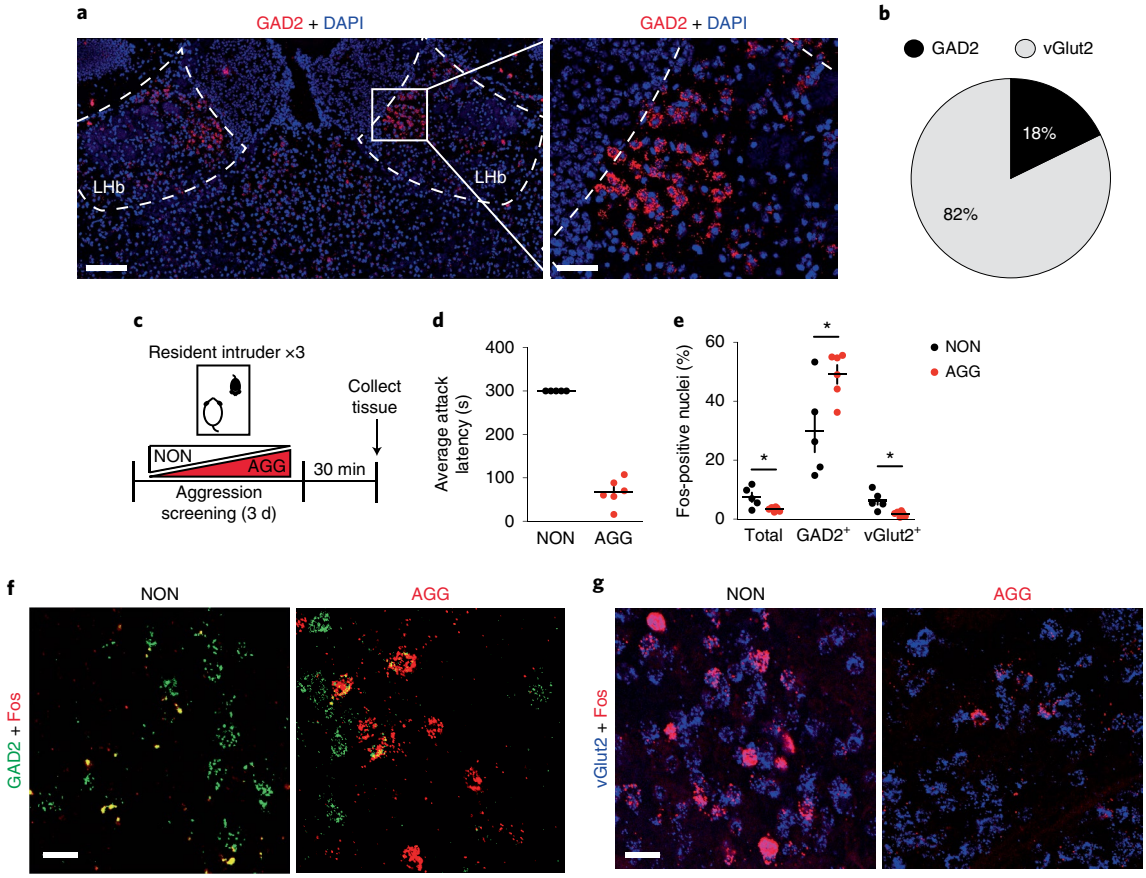

Fig. 2 | Aggressive behaviors are associated with increased expression of Fos mRNA in GAD2 LHb neurons. a, ISH for GAD2 in the LHb (left image scale bar, 150 μm; right image scale bar, 70 μm). Experimental images were taken from three biologically independent mice, two slices per mouse, with similar results obtained. **b**, Pie chart depicting percentage of LHb neurons that are positive for GAD2 or vGlut2 mRNA as determined by ISH, $n = 3$ biologically independent mice. **c**, Experimental timeline for Fos ISH experiments. **d**, Average attack latency for NONs and AGGs over 3 d of RI screening, $n = 6$ biologically independent mice. **e**, Fos-positive nuclei were lower in AGGs than in NONs for total and vGlut2-positive LHb neurons and higher in GAD2-positive LHb neurons (two-tailed Student's *t*-test, $n = 5$ biologically independent NON mice, $n = 6$ biologically independent AGG mice, two slices per mouse, total: $t_9 = 2.828$, $P = 0.0198$; vGlut2: $t_9 = 3.421$, $P = 0.0176$; GAD2: $t_9 = 2.686$, $P = 0.025$). **f**, Representative images of ISH in the LHb for Fos (red) and GAD2 (green) in NON and AGG mice after RI screening (scale bar, 35 μm). Experimental images were obtained from 11 independent mice with two images taken per mouse, with similar results obtained. **g**, Representative images of ISH in the LHb for Fos (red) and vGlut2 (blue) in NON and AGG mice after RI screening (scale bars, 35 μm). Experimental images were obtained from 11 independent mice with two images taken per mouse, with similar results obtained. $^*P < 0.05$. All data are expressed as mean ± s.e.m.

involved in encoding the rewarding properties of aggressive social interactions and the contexts associated with them.

Aggression is associated with increased LHb GAD2 neuron activity. Although the LHb consists predominantly of glutamatergic projection neurons expressing vGlut2 (ref. [16]), GAD2-expressing LHb cells have also been reported[18]. To confirm this, we performed in situ hybridization (ISH) for GAD2 mRNA in the LHb (Fig. 2a,b). We found that GAD2 neurons make up ~18% of total LHb neurons and are localized primarily to the medial aspect of the LHb (Fig. 2b). To better understand the role of specific LHb cell types (that is, GAD2 versus vGlut2) in aggressive behavior, we screened mice in RI and compared the number of Fos-positive GAD2 and vGlut2 nuclei in the LHb of AGGs and NONs (Fig. 2c,d). After the last RI experience, both total Fos-positive nuclei and vGlut2 Fos-positive nuclei were reduced in AGGs compared to NONs (Fig. 2e–g). Interestingly, GAD2 Fos-positive nuclei were increased in AGGs compared to NONs (Fig. 2e–g), suggesting that these cells might be playing a role in regulating aggressive behavior.

To assess the dynamics of GAD2 neurons in real time, we used cell-type-specific fiber photometry to record their activity during RI and aggression CPP (Fig. 3a,b). To do this, we injected AAV-Flex-GCaMP6 into the LHb of GAD2-Cre mice and implanted a fiber above the infected cells. AGGs displayed robust activation of GAD2 neurons around the time at which an aggressive interaction commenced (Fig. 3d,e), whereas GAD2 neuron activity decreased near the time at which they withdrew from an aggressive bout (Fig. 3h,i). These responses were observed on both day 1 and day 3 of RI, and increases in overall GAD2 neuron activity coincided with increases in aggressive behavior (Fig. 3c,l,m and Extended Data Fig. 2). Interestingly, the activity of GAD2 neurons in NONs was only weakly associated with social behavior in RI (Fig. 3f,g,j–k,n–o), indicating that LHb responses to social targets in NONs might not be strongly driven by alterations in the activity of LHb GAD2 neurons. During the aggression CPP test, AGGs displayed increased LHb GAD2 neuron activity in the aggression-paired context compared to the unpaired context (Fig. 3p,q). Although we did not observe any significant differences in LHb GAD2 neuron activity between the paired and unpaired chambers in NONs (Fig. 3r,s), LHb GAD2 neuron activity was correlated with aggression CPP score in both AGGs and NONs (Extended Data Fig. 2). Therefore, our findings imply that LHb GAD2 neurons are

a subpopulation within the LHb whose activity during aggression and exposure to aggression-associated contexts opposes that of the LHb as a whole.

Optogenetic manipulation of LHb GAD2 neurons influences aggression. Although LHb GAD2 neurons have been reported to express GABA as well as the vesicular GABA transporter (vGAT)[18], it remains unknown whether these neurons promote local inhibition within the LHb, outside the LHb or both. To assess whether LHb GAD2 neurons can provide local inhibition, we transduced LHb GAD2 neurons with channel-rhodopsin (ChR2) by injecting AAV-DIO-ChR2 into the LHb of GAD2-Cre mice and applied blue light to brain slices containing the LHb while recording from putative LHb vGlut2 neurons using whole-cell electrophysiology (Fig. 4a). We found that optogenetic stimulation of LHb GAD2 neurons in slice elicited monosynaptic inhibitory currents in non-GAD2 (vGlut2) neurons that were completely blocked with the GABA receptor antagonist picrotocxin (Fig. 4b,c). We did not detect excitatory currents in any neurons as a result of GAD2 neuron optogenetic stimulation, as evidenced from a lack of responses when holding neurons at −70 mV. Moreover, DREADD-mediated activation of LHb GAD2 neurons in vivo reduced the total number of putative non-GAD2 Fos-positive neurons in the LHb (Fig. 4d–g). Together, these data provide the first evidence of a functional inhibitory microcircuit within the LHb and challenge the longstanding notion that the LHb is devoid of local sources of inhibition. To test whether LHb GAD2 neurons project outside of the LHb, we performed anterograde tracing of their projections by injecting AAV-DIO-eYFP into the LHb of GAD2-Cre mice. We did not observe evidence of eYFP-positive axons in primary known LHb target regions, such as the ventral tegmental area (VTA), the dorsal raphe nucleus (DRN), the median raphe nucleus (MRN) or the rostromedial tegmental nucleus (RMTg) (Extended Data Fig. 3). These results suggest that LHb GAD2 neurons are capable of inhibiting neurons within the LHb itself and might not directly target neurons in the major downstream regions of LHb efferents.

To determine whether LHb GAD2 neurons play a functional role in aggressive behavior, we performed in vivo optogenetic manipulation of LHb GAD2 neurons during RI and the aggression CPP test (Fig. 4h). To do this, we injected AAV-DIO-ChR2 or AAV-DIO-eYFP into the LHb of GAD2-Cre mice and implanted a fiber above the LHb. We found that optogenetic activation of GAD2 LHb neurons with ChR2 in AGG mice (20 Hz, 20-ms pulses, 7 mW) reduced the latency to attack and increased the total duration of time spent attacking in RI (Fig. 4i,j). Notably, we were unable to elicit aggression in NONs with optogenetic stimulation of GAD2 neurons (Extended Data Fig. 4). Optogenetic activation of GAD2 LHb neurons in AGGs during the aggression CPP test also increased the time spent in the intruder-paired context (Fig. 4k). However, stimulation of GAD2 neurons did not elicit a real-time place preference (RT-PP) (Fig. 4l) or promote CPP for palatable food (Supplementary Fig. 1). These data imply that GAD2 neurons potentiate aggression by enhancing its rewarding properties but do not modulate food reward or general reward-like responding. Consistent with these findings, consumption of palatable food did not alter the activity of LHb GAD2 neurons as determined using fiber photometry and the calcium sensor GCaMP6 (Supplementary Fig. 1).

To determine if LHb GAD2 neurons are necessary for aggression, we tested whether optogenetic inhibition of them reduces aggression and aggression CPP. To do this, we injected AAV-DIO-NpHR (halo-rhodopsin) or AAV-DIO-eYFP into the LHb of GAD2-Cre mice and implanted a fiber above the LHb. Although this did not completely block aggression, optogenetic inhibition of GAD2 LHb neurons in AGGs (constant light, 8 s on/2 s off, 7 mW) increased the latency to attack and decreased the total duration of time spent attacking in RI (Fig. 4m,n). Optogenetic inhibition of LHb GAD2 neurons also promoted aversion for the intruder-paired context during aggression CPP (Fig. 4o). Together, these results indicate that LHb GAD2 neurons can alter the valence of aggressive social interactions and, subsequently, the intensity of aggression itself.

Orexin modulates LHb GAD2 neurons. Although little is currently known about LHb GAD2 neurons, reports suggest that they express several hypothalamus-derived neuropeptide and hormone receptors, including OxR2 (refs. [17,18]). Orexin has not been previously implicated in aggression but has been implicated in various motivated behaviors, from drug addiction to social interaction[25–29]. Therefore, we hypothesized that orexin-mediated activation of LHb

Fig. 3 | Aggressive behaviors are associated with increased GAD2 LHb neuron activity. a, Surgical manipulations and representative viral infection for LHb GAD2 neuron photometry experiments (scale bar, 400 μm). **b**, Experimental timeline for LHb GAD2 neuron photometry experiments. **c**, AGGs displayed reduced attack latency on day 3 of RI compared to day 1 of RI (one-way repeated-measures ANOVA, $n = 5$ biologically independent mice, $F_{2,10} = 10.78$, $P = 0.0032$, main effect of day; Dunnett's test for multiple comparisons, day 1 versus day 3, adjusted $P = 0.0018$). **d**, Peri-event plot of AGG LHb GAD2 activity 2 s before and after a bite on day 3 of RI. For all peri-event plots, the black line denotes the mean signals for all animals, whereas the blue shaded region denotes the s.e.m., $n = 5$ biologically independent mice, 3–5 bites per mouse. **e**, AGGs displayed an increase in average GAD2 neuron activity after a bite (two-tailed paired t-test, $n = 5$ biologically independent mice, 3–5 bites per mouse, $t_5 = 4.914$, $P = 0.0044$). **f**, Peri-event plot of NON LHb GAD2 neuron activity 2 s before and after an intruder approach on day 3 of RI. The black line denotes the mean signals for all animals, whereas the blue shaded region denotes the s.e.m., $n = 5$ biologically independent mice, 3–5 approaches per mouse. **g**, NONs displayed no change in average LHb activity after an approach (two-tailed paired t-test, $n = 5$ mice, 3–5 approaches per mouse, $t_4 = 2.437$, $P = 0.0714$). **h**, Peri-event plot of AGG LHb GAD2 neuron activity 2 s before and after a withdrawal from an aggressive bout. The black line denotes the mean signals for all animals, whereas the blue shaded region denotes the s.e.m., $n = 6$ biologically independent mice, 3–5 withdrawals per mouse. **i**, AGGs displayed a decrease in average LHb activity after a withdrawal (two-tailed paired t-test, $n = 6$ mice, 3–5 withdrawals per mouse, $t_5 = 3.022$, $P = 0.0294$. **j**, Peri-event plot of NON LHb GAD2 neuron activity 2 s before and after a withdrawal from a non-aggressive social interaction. The black line denotes the mean signals for all animas, whereas the blue shaded region denotes the s.e.m., $n = 5$ biologically independent mice, 3–5 withdrawals per mouse. **k**, NONs displayed no change in LHb GAD2 neuron activity after a withdrawal from a non-aggressive social interaction (two-tailed paired t-test, $n = 5$ biologically independent mice, 3–5 withdrawals per mouse, $t_4 = 1.170$, $P = 0.3068$). **l**, Representative traces of AGG LHb GAD2 neuron activity in the absence and presence of an intruder mouse during day 3 of RI. **m**, AGGs displayed increased GAD2 LHb activity across 3 d of RI (one-way repeated-measures ANOVA, $n = 6$ biologically independent mice, $F_{2,10} = 5.653$, $P = 0.0228$; Dunnett's multiple-comparisons test day 1 versus day 3, adjusted $P = 0.0133$). **n**, Representative traces of NON LHb GAD2 neuron activity in the absence and presence of an intruder mouse during day 3 of RI. **o**, NONs did not display changes in LHb GAD2 neuron activity across 3 d of RI (one-way repeated-measures ANOVA, $n = 5$ mice, $F_{2,14} = 0.8904$, $P = 0.4476$). **p**, Representative trace of AGG LHb GAD2 neuron activity during the aggression CPP task. **q**, AGGs displayed increased LHb GAD2 neuron activity in the paired context compared to the unpaired context during the aggression CPP task (two-tailed paired t-test, $t_4 = 2.885$, $P = 0.0448$). **r**, Representative trace of NON LHb GAD2 neuron activity during the aggression CPP task. **s**, NONs did not display differences in LHb GAD2 neuron activity during the aggression CPP task (two-tailed paired t-test, $t_3 = 0.03591$, $P = 0.9736$). $^*P < 0.05$, $^{**}P < 0.01$. All data are expressed as mean ± s.e.m.

GAD2 neurons via OxR2 would promote aggressive behavior. First, we characterized the expression of OxR2 in the LHb by performing double-fluorescent ISH for OxR2 in GAD2 and vGlut2 neurons (Fig. 5a). We detected expression of OxR2 in nearly 100% of LHb GAD2 neurons, whereas fewer than 10% of LHb vGlut2 neurons were positive for OxR2 (Fig. 5b,c). To visualize orexin-positive

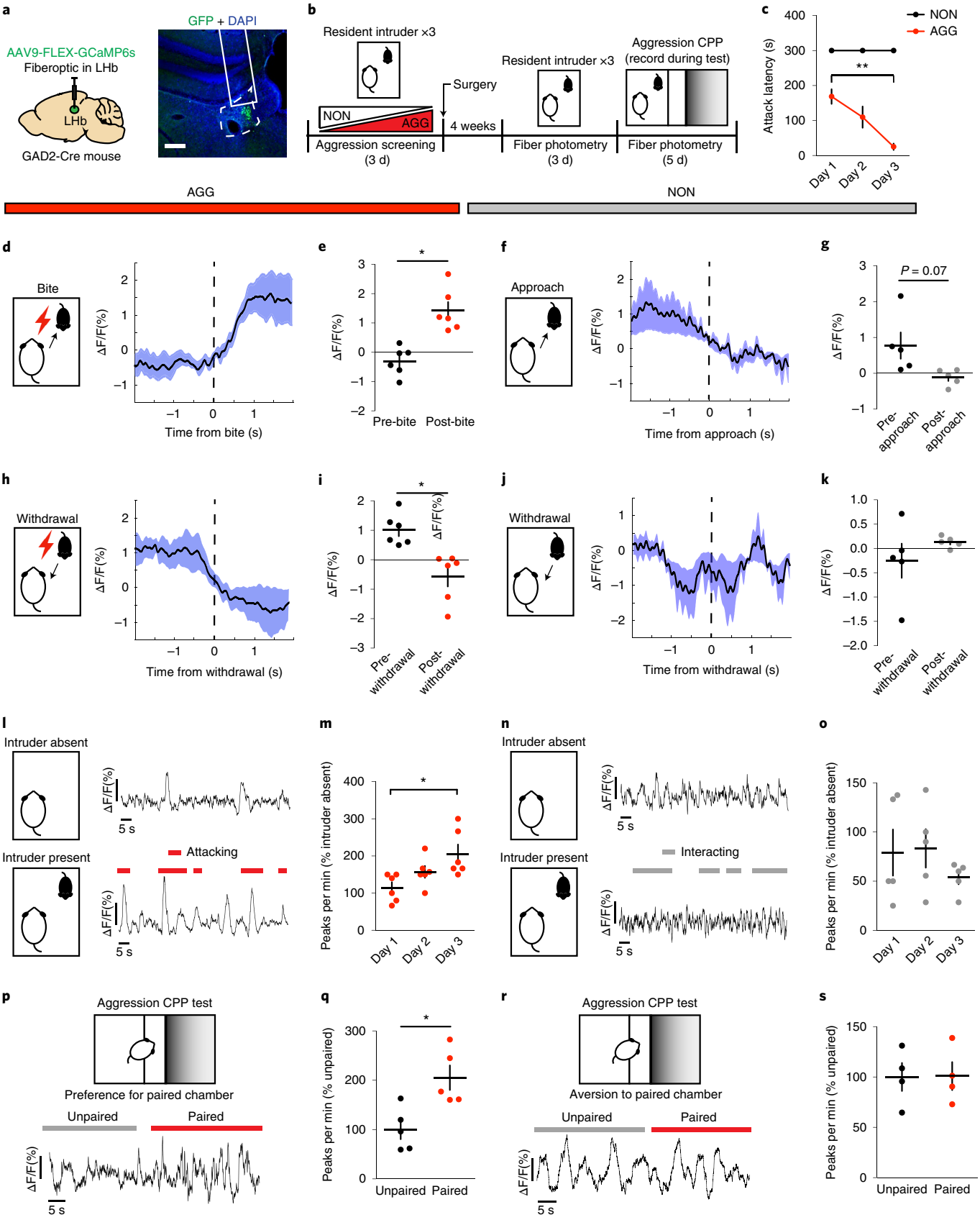

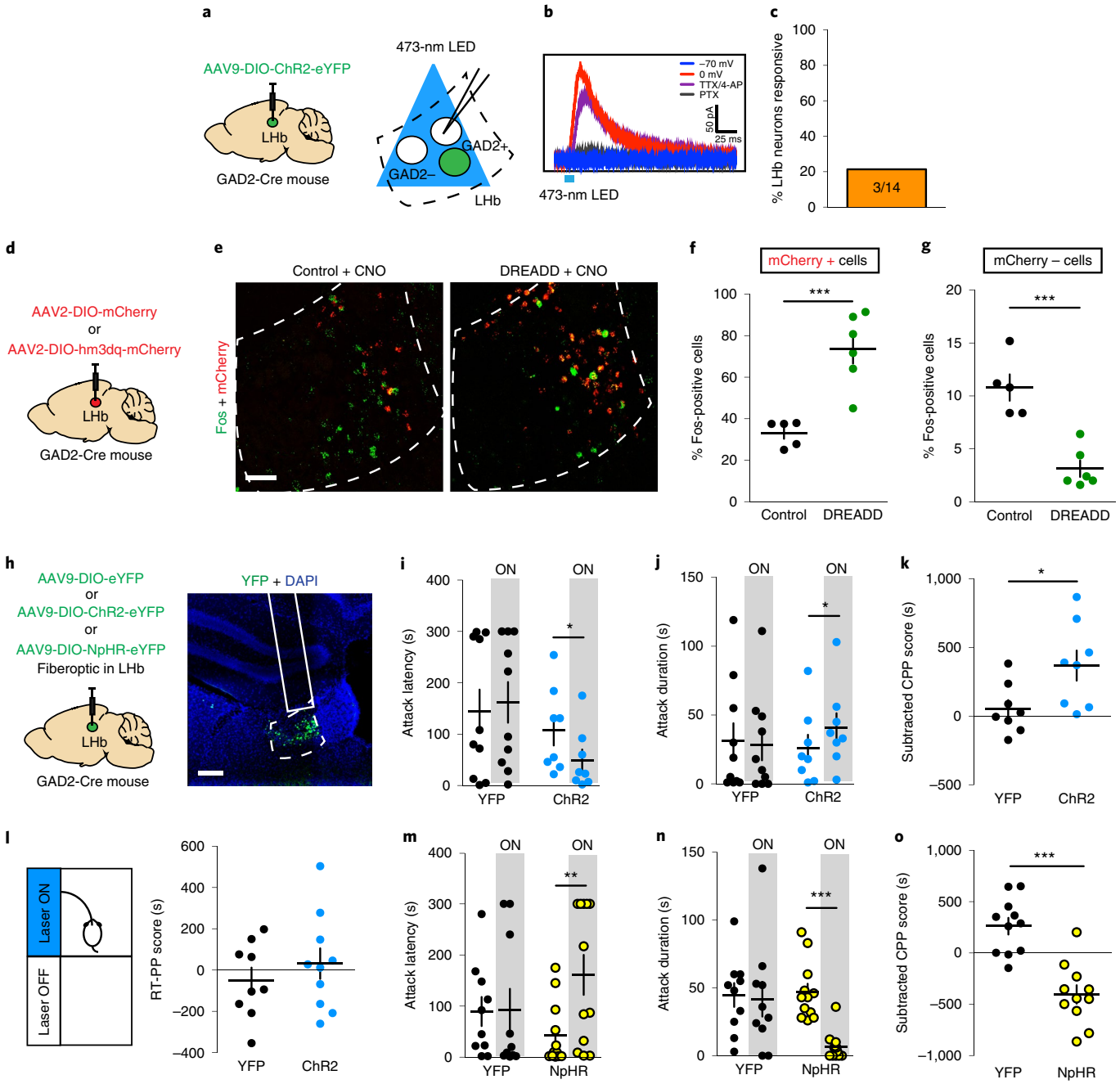

Fig. 4 | GAD2 LHb neurons are locally inhibitory and regulate aggressive behaviors in AGGs. a, Surgical manipulations and experimental schematic for slice optogenetic stimulation of GAD2 LHb neurons. **b**, Representative trace of GFP-negative neurons in response to optogenetic stimulation of nearby GAD2 neurons when cells are held at 0 mV or −70 mV and in the presence of TTX or the GABA receptor antagonist picrotoxin. **c**, Percent LHb GFP-negative neurons responding to optogenetic stimulation of GAD2 neurons. **d**, Surgical manipulations for GAD2 DREADD experiments. **e**, Representative images of ISH for Fos (green) and mCherry (red) mRNA in control and DREADD mice after treatment with CNO (scale bar, 50 μm). **f**, CNO treatment increased the percent of Fos-expressing mCherry-positive neurons in DREADD mice compared to controls (two-tailed Student's *t*-test, $n=5$ biologically independent mice per group, $t_9 = 4.905$, $P=0.0008$). **g**, CNO treatment reduced the percent of Fos-expressing mCherry-negative neurons in DREADD mice compared to controls (two-tailed Student's *t*-test, $n=5$ biologically independent mice per group, $t_9 = 5.439$, $P=0.0004$). **h**, Surgical manipulations and representative viral infection image for in vivo GAD2 LHb neuron optogenetics experiments (scale bar, 300 μm). **i**, ChR2-mediated stimulation of GAD2 LHb neurons reduced attack latency in RI (two-tailed paired *t*-test, $n=8$ biologically independent mice, $t_7 = 3.724$, $P=0.0136$). **j**, ChR2-mediated stimulation of LHb neurons increased attack duration in RI (paired *t*-test, $n=8$ mice, $t_7 = 2.690$, $P=0.0311$). **k**, ChR2-mediated stimulation of GAD2 LHb neurons increased aggression CPP (two-tailed Student's *t*-test, $n=8$ biologically independent mice per group, $t_{14} = 2.482$, $P=0.0264$). **l**, Stimulation of GAD2 LHb neurons did not induce a RT-PP (two-tailed Student's *t*-test, $n=9$ biologically independent mice per group, $t_{17} = 0.8271$, $P=0.4196$). **m**, NpHr-mediated inhibition of GAD2 LHb neurons increased attack latency in RI (two-tailed paired *t*-test, $n=12$ biologically independent mice, $t_{11} = 3.242$, $P=0.0078$). **n**, NpHr-mediated inhibition of GAD2 LHb neurons reduced attack duration in RI (two-tailed paired *t*-test, $n=12$ mice, $t_{11} = 5.504$, $P=0.002$). **o**, NpHr-mediated inhibition of GAD2 LHb neurons reduced aggression CPP (two-tailed Student's *t*-test, $n=11$ mice per group, $t_{20} = 5.517$, $P<0.0001$). $^*P<0.05$, $^{**}P<0.01$, $^{***}P<0.001$. All data are expressed as mean ± s.e.m.

axons in the LHb and their proximity to LHb GAD2 neurons, we used the high-resolution microscopy technique AiryScan in conjunction with viral-mediated fluorescent labeling (AAV-DIO-GFP in GAD2-Cre mice) of GAD2 cells and immunohistochemical (IHC) analysis to visualize orexin axons. After three-dimensional rendering of the images, we observed orexin axons that were closely apposed to GAD2 cell bodies and processes (Extended Data Fig. 5). To functionally test the hypothesis that orexin modulates the activity of GAD2 neurons, we bath-applied orexin to ex vivo brain slices containing the LHb. We found that this increased the firing rate of GAD2 neurons, indicating that they are indeed physiologically activated by orexin (Fig. 5d–f).

To investigate whether LHb OxR2 signaling is implicated in aggression, we screened mice in RI, categorized them as either AGGs or NONs and collected LHb tissue to perform qPCR for *Hcrt2r*, the transcript encoding OxR2. We found that after 3 d of RI, AGGs displayed increased OxR2 expression compared to NONs (Fig. 5g,h and Extended Data Fig. 6). We did not observe this increase after 1 d of RI, suggesting that LHb OxR2 expression increases as a consequence of repeated aggression in RI. Next, we used ISH to label OxR2 mRNA in LHb GAD2 and vGlut2 neurons in AGGs and NONs after 3 d of RI. This was necessary to verify that OxR2 expression increased in GAD2 LHb neurons and to control for the possibility of extra-LHb tissue contamination of tissue punches in our qPCR experiments. As expected, we detected increased OxR2 expression in AGGs compared to NONs specifically in GAD2 neurons, with no change in vGlut2 neuron OxR2 expression (Fig. 5i–k and Extended Data Fig. 6). These data provide support for a model whereby increased orexin signaling in LHb GAD2 neurons as a consequence of repeated aggression experience promotes aggression and its rewarding properties, possibly through increased local inhibition of LHb principal neurons.

Manipulation of orexin signaling in the LHb influences aggression. To assess the effects of orexin on the activation of GAD2 and vGlut2 neurons in the LHb in vivo, we optogenetically stimulated orexin terminals in the LHb of orexin-Cre mice injected with AAV-DIO-ChR2 in the LH and performed ISH for Fos and GAD2 or vGlut2 (Fig. 6a). Optogenetic stimulation of orexin terminals in the LHb (20 Hz, 20-ms pulses, 7 mW for 30 min) reduced total LHb Fos expression as well as Fos expression in vGlut2-positive LHb neurons, whereas it increased Fos expression in GAD2 neurons compared to mice that received the AAV-DIO-eYFP control virus (Fig. 6b–d). Consistent with a decrease in overall Fos expression observed in the LHb after orexin terminal stimulation, systemic administration of selective OxR2 antagonist *N*-ethyl-2-[(6-methoxy-3-pyridinyl)[(2-methylphenyl)sulfonyl]amino]-*N*-(3-pyridinylmethyl)-acetamide (EMPA; 30 mg kg^{-1} intraperitoneal) increased the activity of the LHb as measured by fiber photometry in mice expressing a nonconditional AAV-GCaMP6 in the LHb (Extended Data Fig. 7). It also reduced aggression and aggression CPP without affecting locomotion or anxiety-like behavior (Extended Data Fig. 7). Together, these results provide further support for our model and suggest that locally inhibitory LHb GAD2 neurons are activated by orexin from the LH.

Next, we tested whether orexin inputs to the LHb play a functional role in aggression and aggression reward. To do this, we injected AAV-DIO-ChR2 into the LH of orexin-Cre mice and implanted a fiber above the LHb (Fig. 6e). Optogenetic stimulation of orexin terminals in the LHb (20 Hz, 20-ms pulses, 7 mW) promoted aggression and modestly increased aggression CPP in AGGs (Fig. 6f–h). However, optogenetic stimulation of orexin inputs to the LHb was not sufficient to initiate aggression in NONs (Extended Data Fig. 4). To confirm that these behavioral effects in AGGs were mediated by OxR2, we performed optogenetic stimulation of LHb orexin terminals in mice expressing a microRNA against OxR2 (AAV-miR-OxR2) in the LHb. Stimulation of LHb orexin terminals under these conditions did not alter aggressive behavior (Extended Data Fig. 8). To determine whether inhibition of orexin terminals in the LHb reduces aggressive behavior, we injected AAV-DIO-NpHr in the LH of orexin-Cre mice and implanted a fiber above the LHb. Optogenetic inhibition of LHb orexin terminals indeed reduced aggression and aggression CPP in AGGs (Fig. 6i–k) but did not affect aggression in NONs (Extended Data Fig. 4). Together, these data indicate that orexin signaling in the LHb modulates aggression as well as its rewarding properties via an OxR2-dependent mechanism.

To assess whether OxR2 signaling in LHb GAD2 neurons is necessary for inter-male aggression, we performed cell-type-specific knockdown of OxR2 in GAD2 neurons using a microRNA-based approach (Fig. 7a,b and Extended Data Fig. 9). Knockdown of OxR2 in LHb GAD2 neurons reduced aggression and aggression CPP (Fig. 4m–o), recapitulating the behavioral effects of direct NpHR-mediated inhibition of GAD2 LHb neurons (Fig. 7c–e). Notably, knockdown of OxR2 in GAD2 neurons did not alter locomotor behavior or time spent in the center of an open field, indicating that effects of this manipulation on aggression were not mediated by changes in overall activity or anxiety (Supplementary Fig. 2). Consistent with our previous findings, overexpression of OxR2 in LHb GAD2 neurons did not promote aggressive behavior in NONs (Extended Data Figs. 4 and 10). These data support the conclusion that OxR2 signaling in LHb GAD2 neurons is involved in regulating the reinforcing properties of aggression but not its initiation.

Discussion

Current understanding of the neural circuitry and molecular mechanisms that regulate aggression and that might drive heightened aggression remains incomplete. In this study, we used a

Fig. 5 | Characterization of an LHb orexin circuit. a, Representative ISH images showing OxR2 expression in GAD2 and vGlut2 LHb neurons (scale bar, 20 µm). **b**, OxR2 is expressed primarily in GAD2 neurons compared to vGlut2 neurons (two-tailed Student's *t*-test, $n=3$ biologically independent mice, 1–2 slices per mouse, $t_4 = 15.67$, $P < 0.0001$). **c**, GAD2 neurons express more OxR2 mRNA than vGlut2 neurons (two-tailed Student's *t*-test, $n=3$ biologically independent mice, 1–2 slices per mouse, $t_4 = 15.67$, $P < 0.0001$). **d**, Surgical manipulations and experimental schematic for orexin bath application experiments. **e**, Representative traces from a GFP-positive neuron (GAD2 neuron) during baseline (top), orexin-A (middle) and washout (bottom) conditions. **f**, Orexin bath application increased the firing rate of GFP-positive neurons (Kruskal–Wallis one-way ANOVA with repeated measures, $n=6$ biologically independent mice, $n=9$ cells, Kruskal–Wallis statistic = 7.115, $P=0.0285$; Dunn's multiple-comparisons baseline versus orexin-A, adjusted $P=0.0456$). **g**, Experimental timeline for LHb qPCR experiments. **h**, After 3 d of RI, AGGs expressed significantly more LHb OxR2 mRNA than NONs did (3-d RI: two-tailed Student's *t*-test, $n=7$ biologically independent NON mice, $n=8$ biologically independent AGG mice, $t_{13} = 2.496$, $P=0.0268$; 1-d RI: two-tailed Student's *t*-test, $n=9$ biologically independent NON mice, $n=7$ biologically independent AGG mice, $t_{14} = 0.1433$, $P=0.881$). **i**, Experimental timeline for OxR2 ISH experiments. **j**, After 3 d of RI, AGGs displayed increased GAD2 neuron OxR2 mRNA compared to NONs (two-tailed Student's *t*-test, $n=5$ biologically independent NON mice, $n=6$ biologically independent AGG mice, GAD2 neurons: $t_9 = 6.039$, $P=0.0002$; vGlut2 neurons: $t_9 = 0.6735$, $P=0.5175$). **k**, Representative images of ISH for OxR2 and GAD2, in AGGs and NONs after 3 d of RI (scale bar, 20 µm). Experimental images were obtained from 11 independent mice with two slices imaged per mouse, with similar results obtained. $^*P<0.05$, $^{***}P<0.001$ All data are expressed as mean ± s.e.m.

multidisciplinary approach to monitor, manipulate and functionally map a previously uncharacterized inhibitory cell type in the LHb that may influence the expression of aggression by altering its rewarding properties. This cell type is under modulatory control by the neuropeptide orexin, which appears to influence its capacity to promote aggression and preference for aggression-paired contexts.

Our results using in vivo fiber photometry to measure neural activity provide important new information regarding the dynamics of LHb activity during aggression and highlight adaptations that occur in LHb neurons as a result of previous fight experience. We demonstrated that attacks are time-locked to reductions in overall LHb activity, which agrees with previous studies showing that functional inhibition of LHb neurons can enhance aggression and

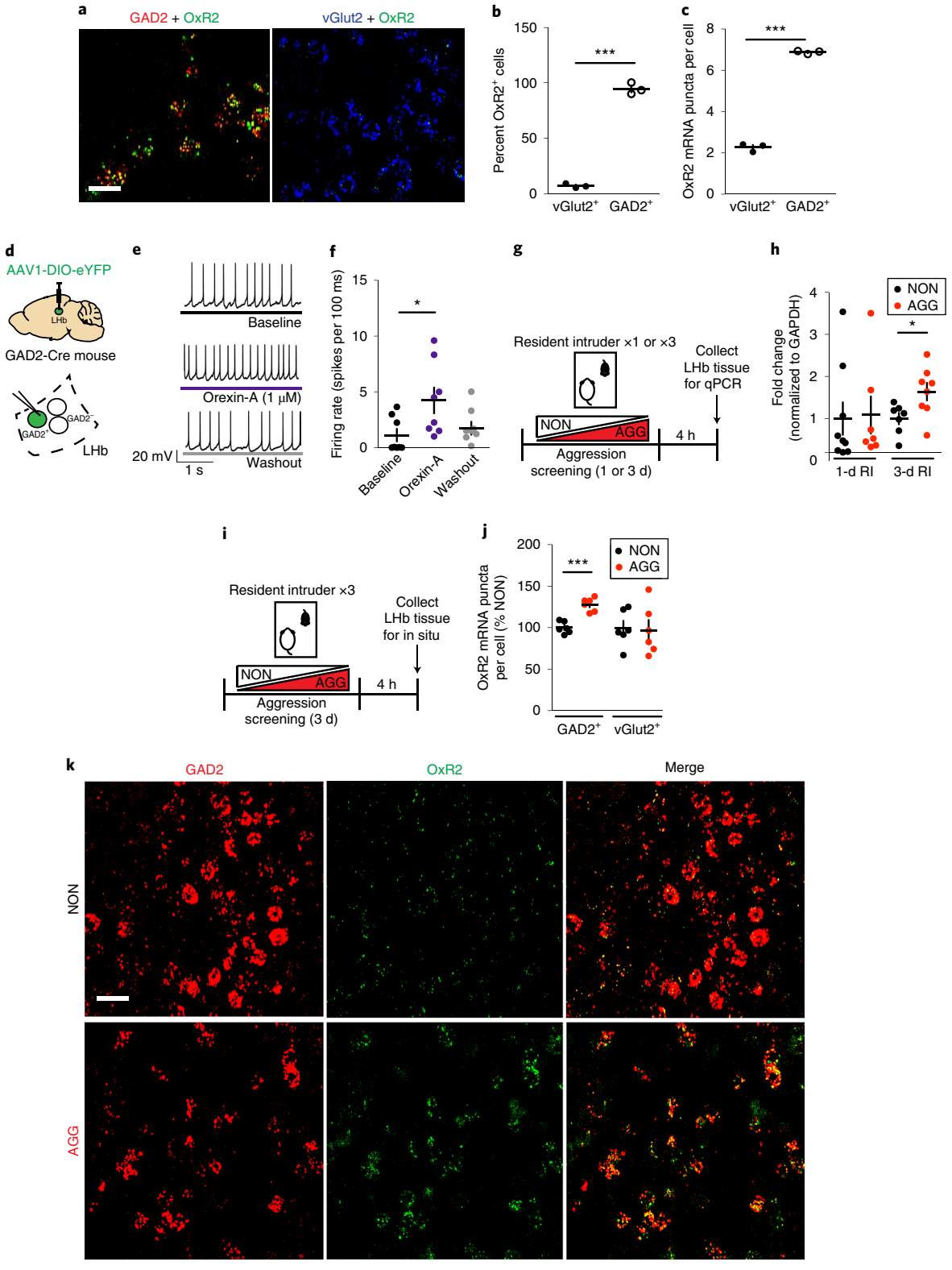

its rewarding properties[9,15]. Furthermore, as AGGs learn to associate particular contexts with aggressive social interactions involving submissive intruders, the LHb displays reduced activity in these contexts even in the absence of the intruder, suggesting that the structure encodes information about the rewarding properties of aggression and aggression-paired contexts on the basis of previous experience. These findings are consistent with recent reports describing plasticity in LHb neurons as animals learn to associate cues predicting aversive or rewarding stimuli[28,29]. Although activity of the LHb as a whole might be reduced during aggression or in response to aggression-related cues, we identified a small subset of GAD2-expressing LHb neurons that show robust activation on a similar timescale to the whole LHb. This suggests that multiple LHb cell types, not glutamatergic LHb projection neurons alone, are important for the modulation of aggression and its rewarding properties.

Our study provides the first evidence that GAD2 neurons in the LHb suppress the activity of principal neurons within the LHb that, when active, typically encode aversion. This finding brings into question the currently accepted model of LHb microcircuit as being purely excitatory by adding a new element of inhibitory regulation within the LHb. However, many questions about these neurons remain. First, do LHb GAD2 neurons release neuropeptides or other neurotransmitters besides GABA? Notably, we found no evidence of excitatory (glutamatergic) currents in LHb principal neurons elicited by GAD2 neuron stimulation (Fig. 4a,b), but this does not preclude the possibility that other messengers are also released from these neurons. In fact, a recent study that performed single-cell sequencing of LHb neurons found that cells expressing GAD2 might also express transcripts encoding precursors for neuropeptides, such as pituitary adenylate cyclase-activating polypeptide and enkephalin[17]. Future studies should aim to verify coexpression of GAD2 and these neuropeptide precursors. Second, the question remains whether LHb GAD2 neurons exert broad inhibitory control over LHb projection neurons in aggression, or whether there is projection-specific connectivity. Notably, two major outputs of the LHb—the DRN and the VTA—were previously implicated in aggressive behavior[30,31], but the role of each of these target regions in controlling motivational aspects of aggression, such as preference for aggression-paired contexts, remains poorly understood. Future investigations should attempt to map the intra- and extra-LHb targets of GAD2 neurons that are important for regulating aggression. Third, what role, if any, do other inputs to LHb GAD2 neurons play in aggression? In addition to expressing OxR2, LHb GAD2 neurons have also been shown to express estrogen and vasopressin receptors[18], both of which were implicated previously in aggression[32,33]. It is also possible that other brain areas implicated in aggression regulation and projecting to the LHb, such as the prefrontal cortex[34] and the lateral septum[35], target LHb GAD2 neurons directly to regulate aggression, and this should also be tested in future studies.

Our results suggest that, in the context of appetitive aggression, LHb GAD2 neurons both encode reward-related signals at the completion of attacks and promote future attacks. This is not unlike previous reports that VTA dopamine neurons both encode reward-related signals after the initiation of prosocial interactions and promote future pro-social interactions[36]. The fact that optogenetic stimulation of LHb GAD2 neurons enhanced aggression in AGGs but did not elicit aggression in NONs suggests that LHb GAD2 neurons are not mediating attack initiation in this context. However, we know from our CPP studies that activity in LHb GAD2 neurons enhances seeking behavior for aggression-associated contexts. Thus, we propose that optogenetic stimulation of LHb GAD2 neurons during RI enhances the perceived reward magnitude of each attack, such that the drive to carry out subsequent attacks is enhanced through repeated positive reinforcement. This might ultimately involve feedback connections between reward centers downstream of the LHb such as the VTA and aggression-initiation centers such as the ventromedial hypothalamus (VMH) and medial amygdala. For example, by providing local inhibition to LHb principal neurons, GAD2 neurons might effectively disinhibit the VTA, thus encoding signals to preempt future aggressive behavior. Considering how little we know about these GAD2 neurons and their role in behavior, an important question is whether they play a wider role in LHb-mediated behaviors. Although we know from our current data that LHb GAD2 neurons promote aggression CPP without altering food CPP or RT-PP, it seems unlikely that they broadly promote reward-related behavior. However, future studies will need to test the role of LHb GAD2 neurons in response to additional rewarding stimuli, such as addictive drugs or prosocial interactions. We also did not assess the role of LHb GAD2 neurons in other well-established LHb-regulated behaviors, such as passive, active or learned aversive behaviors[37]. Future studies to address the broader behavioral role of these LHb GAD2 neurons are necessary.

As stated above, we provide evidence that LHb GAD2 neurons regulate aggression reward through orexin receptor signaling, which is consistent with studies demonstrating a role for orexin in other motivated behaviors. For example, several groups showed that inhibition of orexin signaling reduces CPP, self-administration and relapse for drugs of abuse[22,25,26,38–40]. In addition, orexin neurons are activated by cues and contexts associated with natural rewards like food[41] and sex[42]. Thus, we were surprised to find that activation of LHb GAD2 neurons did not potentiate, or disrupt, the preference displayed during the testing phase of our palatable food CPP assay (Supplementary Fig. 6). Although projections from LH glutamate neurons to the LHb indeed affect feeding behaviors[43], these might

Fig. 6 | Optogenetic manipulation of orexin inputs to the LHb modulates aggressive behavior in AGGs. a, Surgical manipulations and experimental timeline for optogenetic stimulation of orexin terminals in the LHb followed by ISH for Fos, GAD2 and vGlut2. **b**, Optogenetic stimulation of orexin terminals in the LHb increased Fos in GAD2 neurons and decreased Fos in vGlut2 neurons and DAPI-positive cells (two-tailed Student's *t*-test, $n=5$ biologically independent mice per group, two slices per mouse; GAD2: $t_8 = 3.854$, $P=0.0048$; vGlut2: $t_8 = 3.236$, $P=0.0120$; DAPI: $t_8 = 2.340$, $P=0.0475$). **c**, Representative images of Fos expression in LHb GAD2 neurons from YFP and ChR2 mice (scale bar, 40 μm). Experimental images were obtained from ten mice, two slices per mouse, with similar results obtained. **d**, Representative images of Fos expression in LHb vGlut2 neurons from YFP and ChR2 mice (scale bar, 40 μm). Experimental images were obtained from ten mice, two slices per mouse, with similar results. **e**, Surgical manipulations and representative viral infection images for optogenetic manipulation of orexin terminals in the LHb (scale bar, 150 μm). **f**, Optogenetic stimulation of orexin terminals reduced attack latency in RI (NpHr, two-tailed paired *t*-test, $n=10$ biologically independent mice, $t_9 = 2.354$, $P=0.043$). **g**, Optogenetic stimulation of LHb orexin terminals increased attack duration in RI (NpHr, two-tailed paired *t*-test, $n=10$ biologically independent mice, $t_9 = 2.335$, $P=0.0444$). **h**, Optogenetic stimulation of LHb orexin terminals did not significantly increase aggression CPP (two-tailed Student's *t*-test, $n=10$ biologically independent mice per group, $t_{18} = 1.642$, $P=0.1140$). **i**, Optogenetic inhibition of LHb orexin terminals increased attack latency in RI (NpHr, two-tailed paired *t*-test, $n=8$ biologically independent mice, $t_7 = 6.671$, $P=0.0003$). **j**, Optogenetic inhibition of LHb orexin terminals reduced attack duration in RI (NpHr, two-tailed paired *t*-test, $n=8$ biologically independent mice, $t_7 = 4.252$, $P=0.0038$). **k**, Optogenetic inhibition of LHb orexin terminals reduced aggression CPP (two-tailed Student's *t*-test, $n=11$ YFP, $n=10$ NpHr, $t_{19} = 2.993$, $P=0.0085$). $^*P<0.05$, $^{**}P<0.01$, $^{***}P<0.001$. All data are expressed as mean ± s.e.m.

be non-orexinergic glutamate neurons. Instead, LH orexin neurons might primarily influence feeding behavior through projections to regions outside the habenula, including the VTA[22]. Notably, orexin neurons receive inputs from neurons in the VMH, a region shown to be essential for initiating inter-male attack behavior in mice[41,44]. Thus, LH–LHb orexin neurons might form a link between hypothalamic attack centers and circuits controlling motivation. It will be important in future studies to investigate whether orexin

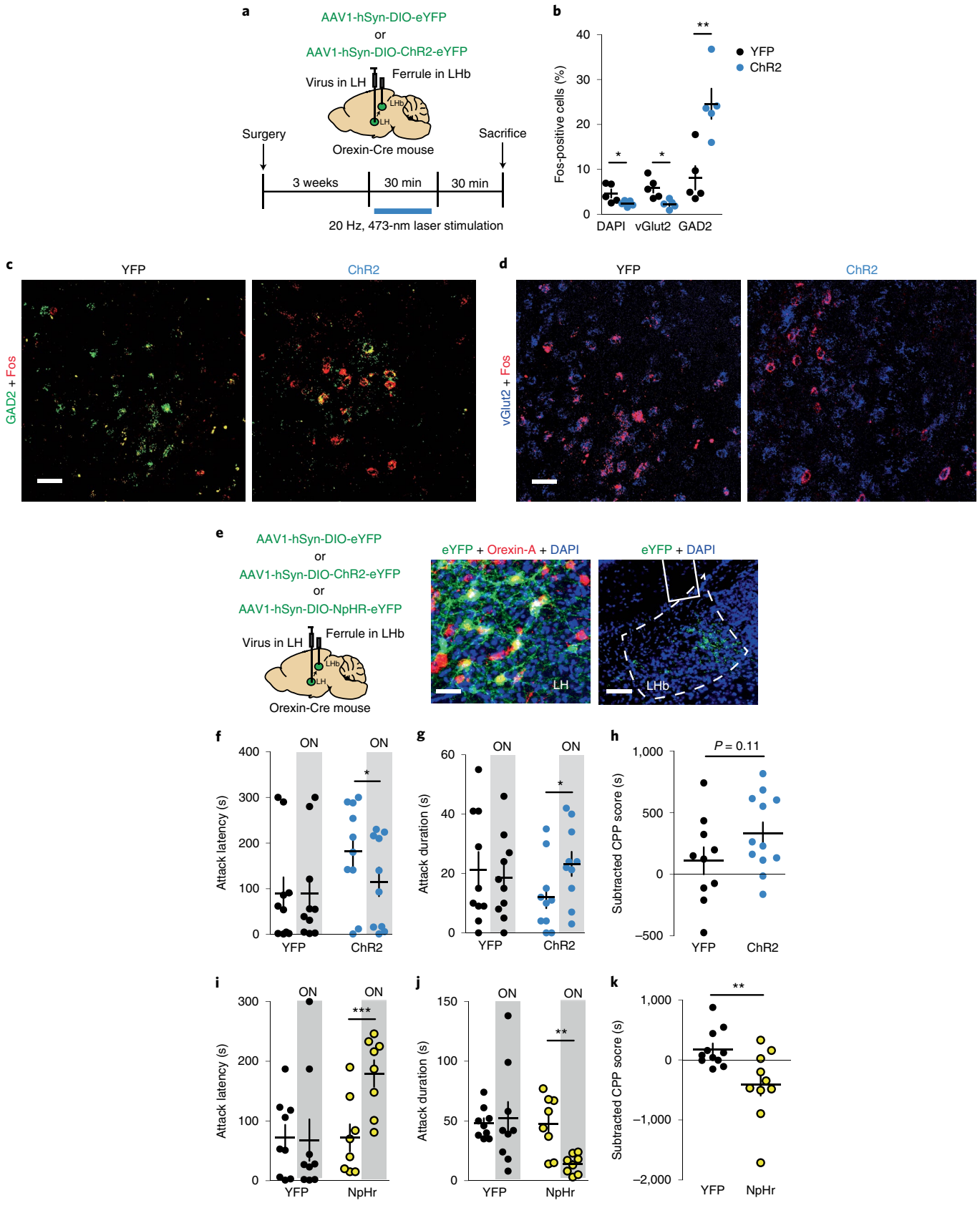

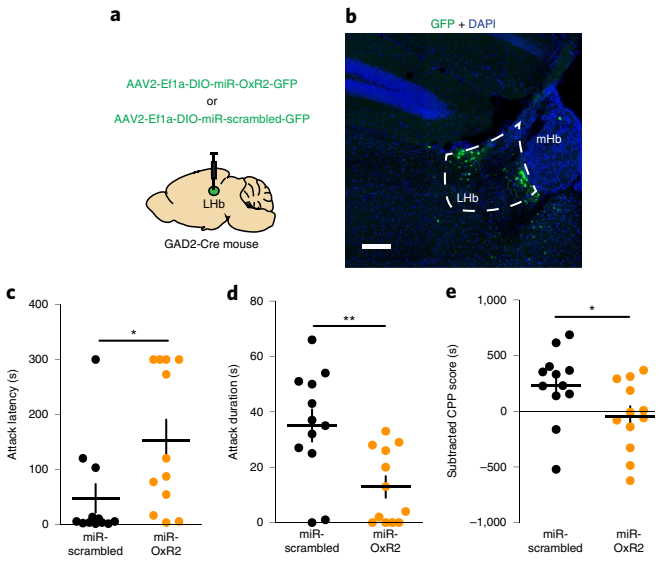

Fig. 7 | Knockdown of OxR2 in GAD2 LHb modulates aggressive behavior in AGGs. a, Surgical manipulations for GAD2 neuron-specific knockdown of OxR2 in the LHb. **b**, Representative viral infection for GAD2 neuron-specific knockdown of OxR2 in the LHb (scale bar, 300 µm). **c**, OxR2 knockdown in GAD2 LHb neurons increased attack latency in RI (two-tailed Student's *t*-test, $n = 12$ biologically independent mice per group, $t_{22} = 2.322$, $P = 0.0299$). **d**, OxR2 knockdown in GAD2 LHb neurons reduced attack duration in RI (two-tailed Student's *t*-test, $n = 12$ biologically independent mice per group, $t_{22} = 3.183$, $P = 0.0043$). **e**, OxR2 knockdown in GAD2 LHb neurons reduced aggression CPP (two-tailed Student's *t*-test, $n = 12$ biologically independent mice per group, $t_{22} = 2.155$, $P = 0{,}0424$). $^{*}P < 0.05$, $^{**}P < 0.01$. All data are expressed as mean ± s.e.m.

neurons projecting to areas other than the LHb are also important for regulating aggression and its rewarding properties and whether the other known orexin receptor, OxR1, plays any role.

In addition to demonstrating that cell-type-specific knockdown of OxR2 reduces aggression and preference for aggression-paired contexts without affecting locomotor behavior, we also found that systemic administration of the OxR2 antagonist EMPA reduces aggression and preference for aggression-paired contexts without affecting locomotor behavior or anxiety-like behavior in the open field test. The lack of an effect of EMPA on locomotion is somewhat surprising, because decades of research have shown that orexin signaling is integral for promoting wakefulness. Indeed, brain-wide deletion of OxR2 (ref. [45]) results in narcolepsy-like phenotypes in rodents. In addition, the dual orexin receptor antagonist suvorexant is currently a US Food and Drug Administration-approved treatment for insomnia, as it aids in the transition from wakefulness to sleep in humans[46]. Although previous studies have shown that 30 mg kg^{-1} EMPA (the concentration used in the current study) reduces spontaneous locomotion in rats[47], it does not in mice[48]. Together with our findings, these data suggest that, at low doses, EMPA might be able to reduce aggression without side effects on arousal. However, given that spontaneous locomotor activity is not a particularly sensitive assay for arousal, this possibility must be examined in detail in future studies.

It is important to note that these experiments were performed during the light phase, which is a period of lower activity levels for nocturnal rodents such as mice. Although the mechanism is not fully elucidated, aggressive behaviors do show variability across the light–dark cycle[49]. As the LHb itself exhibits circadian variations in activity, it is possible that the time of day could affect the extent to which the LHb regulates aggressive behavior[50]. Future studies should assess whether the phase of the light–dark cycle influences the role of the LHb, and the orexinergic LH-to-LHb GAD2 neuron projection, in the regulation of aggression.

In conclusion, we show that orexin plays an important role in modulating aggression and preference for aggression-paired contexts through the activation of inhibitory LHb GAD2 neurons. These findings might have implications for the treatment of exaggerated aggression in some patients with psychiatric disorders.

Online content

Any methods, additional references, Nature Research reporting summaries, source data, extended data, supplementary information, acknowledgements, peer review information; details of author contributions and competing interests; and statements of data and code availability are available at https://doi.org/10.1038/s41593-020-0617-7.

Received: 23 August 2018; Accepted: 2 March 2020;
Published online: 13 April 2020

References

1. Hill, A. P. et al. Aggressive behavior problems in children with autism spectrum disorders: prevalence and correlates in a large clinical sample. *Res. Autism Spectr. Disord.* **8**, 1121–1133 (2014).
2. Cha, J. et al. Neural correlates of aggression in medication-naive children with ADHD: multivariate analysis of morphometry and tractography. *Neuropsychopharmacology* **40**, 1717–1725 (2015).
3. Anderson, N. E. & Kiehl, K. A. Psychopathy and aggression: when paralimbic dysfunction leads to violence. *Curr. Top. Behav. Neurosci.* **17**, 369–393 (2014).
4. Miles, S. R., Menefee, D. S., Wanner, J., Teten Tharp, A. & Kent, T. A. The relationship between emotion dysregulation and impulsive aggression in veterans with posttraumatic stress disorder symptoms. *J. Interpers. Violence* **31**, 1795–1816 (2016).
5. May, M. E. Aggression as positive reinforcement in people with intellectual disabilities. *Res. Dev. Disabil.* **32**, 2214–2224 (2011).
6. Moran, J. K., Weierstall, R. & Elbert, T. Differences in brain circuitry for appetitive and reactive aggression as revealed by realistic auditory scripts. *Front. Behav. Neurosci.* **8**, 425 (2014).
7. Nell, V. Cruelty's rewards: the gratifications of perpetrators and spectators. *Behav. Brain Sci.* **29**, 211–224; discussion 224–257 (2006).
8. Falkner, A. L., Grosenick, L., Davidson, T. J., Deisseroth, K. & Lin, D. Hypothalamic control of male aggression-seeking behavior. *Nat. Neurosci.* **19**, 596–604 (2016).
9. Golden, S. A. et al. Basal forebrain projections to the lateral habenula modulate aggression reward. *Nature* **534**, 688–692 (2016).
10. Flanigan, M., Aleyasin, H., Takahashi, A., Golden, S. A. & Russo, S. J. An emerging role for the lateral habenula in aggressive behavior. *Pharmacol. Biochem. Behav.* **162**, 79–86 (2017).
11. Matsumoto, M. & Hikosaka, O. Lateral habenula as a source of negative reward signals in dopamine neurons. *Nature* **447**, 1111–1115 (2007).
12. Baker, P. M. et al. The lateral habenula circuitry: reward processing and cognitive control. *J. Neurosci.* **36**, 11482–11488 (2016).
13. Lawson, R. P. et al. Disrupted habenula function in major depression. *Mol. Psychiatry* **22**, 202–208 (2017).
14. Ranft, K. et al. Evidence for structural abnormalities of the human habenular complex in affective disorders but not in schizophrenia. *Psychol. Med.* **40**, 557–567 (2010).
15. Chou, M. Y. et al. Social conflict resolution regulated by two dorsal habenular subregions in zebrafish. *Science* **352**, 87–90 (2016).
16. Brinschwitz, K. et al. Glutamatergic axons from the lateral habenula mainly terminate on GABAergic neurons of the ventral midbrain. *Neuroscience* **168**, 463–476 (2010).
17. Hashikawa, Y., et al. Transcriptional and spatial resolution of cell types in the mammalian habenula. Preprint at *bioRxiv* https://doi.org/10.1101/772376 (2019).
18. Zhang, L. et al. A GABAergic cell type in the lateral habenula links hypothalamic homeostatic and midbrain motivation circuits with sex steroid signaling. *Transl. Psychiatry* **8**, 50 (2018).
19. Peyron, C. et al. Neurons containing hypocretin (orexin) project to multiple neuronal systems. *J. Neurosci.* **18**, 9996–10015 (1998).
20. Tsunematsu, T., et al. Acute optogenetic silencing of orexin/hypocretin neurons induces slow-wave sleep in mice. *J. Neurosci.* **31**, 10529–10539 (2011).
21. Blouin, A. M. et al. Human hypocretin and melanin concentrating hormone levels are linked to emotion and social interaction. *Nat. Commun.* **4**, 1547 (2013).
22. Harris, G. C., Wimmer, M. & Aston-Jones, G. A role for lateral hypothalamic orexin neurons in reward seeking. *Nature* **437**, 556–559 (2005).

23. Muschamp, J. W. et al. Hypocretin (orexin) facilitates reward by attenuating the antireward effects of its cotransmitter dynorphin in ventral tegmental area. *Proc. Natl Acad. Sci. USA* **111**, E1648–E1655 (2014).
24. Quarta, D. & Smolders, I. Rewarding, reinforcing and incentive salient events involve orexigenic hypothalamic neuropeptides regulating mesolimbic dopaminergic neurotransmission. *Eur. J. Pharm. Sci.* **57**, 2–10 (2014).
25. Richardson, K. A. & Aston-Jones, G. Lateral hypothalamic orexin/hypocretin neurons that project to VTA are differentially activated with morphine preference. *J. Neurosci.* **32**, 3809–3817 (2012).
26. Tung, L. W. et al. Orexins contribute to restraint stress-induced cocaine relapse by endocannabinoid-mediated disinhibition of dopaminergic neurons. *Nat. Commun.* **7**, 12199 (2016).
27. Schwartzer, J. J., Ricci, L. A. & Melloni, R. H. Jr. Prior fighting experience increases aggression in Syrian hamsters: implications for a role of dopamine in the winner effect. *Aggress. Behav.* **39**, 290–300 (2013).
28. Trusel, M. et al. Punishment-predictive cues guide avoidance through potentiation of hypothalamus-to-habenula synapses. *Neuron* **102**, 120–127.e4 (2019).
29. Lazaridis, I., et al. A hypothalamus-habenula circuit controls aversion. *Mol. Psychiatry* **24**, 1351–1368 (2019).
30. Takahashi, A. et al. Glutamate input in the dorsal raphe nucleus as a determinant of escalated aggression in male mice. *J. Neurosci.* **35**, 6452–6463 (2015).
31. Yu, Q. et al. Dopamine and serotonin signaling during two sensitive developmental periods differentially impact adult aggressive and affective behaviors in mice. *Mol. Psychiatry* **19**, 688–698 (2014).
32. Wersinger, S. R., Ginns, E. I., O'Carroll, A. M., Lolait, S. J. & Young Iii, W. S. Vasopressin V1b receptor knockout reduces aggressive behavior in male mice. *Mol. Psychiatry* **7**, 975 (2002).
33. Ogawa, S. et al. Abolition of male sexual behaviors in mice lacking estrogen receptors α and β (αβERKO). *Proc. Natl Acad. Sci. USA* **97**, 14737–14741 (2000).
34. Takahashi, A., Nagayasu, K., Nishitani, N., Kaneko, S. & Koide, T. Control of intermale aggression by medial prefrontal cortex activation in the mouse. *PLoS ONE* **9**, e94657 (2014).
35. Wong, L. C. et al. Effective modulation of male aggression through lateral septum to medial hypothalamus projection. *Curr. Biol.* **26**, 593–604 (2016).
36. Gunaydin, L. A. et al. Natural neural projection dynamics underlying social behavior. *Cell* **157**, 1535–1551 (2014).
37. Proulx, C. D., Hikosaka, O. & Malinow, R. Reward processing by the lateral habenula in normal and depressive behaviors. *Nat. Neurosci.* **17**, 1146–1152 (2014).
38. Gentile, T. A. et al. Suvorexant, an orexin/hypocretin receptor antagonist, attenuates motivational and hedonic properties of cocaine. *Addict. Biol.* **23**, 247–255 (2018).
39. Sartor, G. C. & Aston-Jones, G. S. A septal–hypothalamic pathway drives orexin neurons, which is necessary for conditioned cocaine preference. *J. Neurosci.* **32**, 4623–4631 (2012).
40. Shoblock, J. R. et al. Selective blockade of the orexin-2 receptor attenuates ethanol self-administration, place preference, and reinstatement. *Psychopharmacology* **215**, 191–203 (2011).
41. Gonzalez, J. A., Iordanidou, P., Strom, M., Adamantidis, A. & Burdakov, D. Awake dynamics and brain-wide direct inputs of hypothalamic MCH and orexin networks. *Nat. Commun.* **7**, 11395 (2016).
42. Muschamp, J. W., Dominguez, J. M., Sato, S. M., Shen, R. Y. & Hull, E. M. A role for hypocretin (orexin) in male sexual behavior. *J. Neurosci.* **27**, 2837–2845 (2007).
43. Stamatakis, A. M. et al. Lateral hypothalamic area glutamatergic neurons and their projections to the lateral habenula regulate feeding and reward. *J. Neurosci.* **36**, 302–311 (2016).
44. Lin, D. et al. Functional identification of an aggression locus in the mouse hypothalamus. *Nature* **470**, 221–226 (2011).
45. Chemelli, R. M. et al. Narcolepsy in orexin knockout mice: molecular genetics of sleep regulation. *Cell* **98**, 437–451 (1999).
46. Herring, W. J. et al. Suvorexant in patients with insomnia: results from two 3-month randomized controlled clinical trials. *Biol. Psychiatry* **79**, 136–148 (2016).
47. Malherbe, P. et al. Biochemical and behavioural characterization of EMPA, a novel high-affinity, selective antagonist for the OX(2) receptor. *Br. J. Pharmacol.* **156**, 1326–1341 (2009).
48. Beig, M. I., Dampney, B. W. & Carrive, P. Both Ox1r and Ox2r orexin receptors contribute to the cardiovascular and locomotor components of the novelty stress response in the rat. *Neuropharmacology* **89**, 146–156 (2015).
49. Todd, W. D. et al. A hypothalamic circuit for the circadian control of aggression. *Nat. Neurosci.* **21**, 717–724 (2018).
50. Mendoza, J. Circadian neurons in the lateral habenula: clocking motivated behaviors. *Pharmacol. Biochem. Behav.* **162**, 55–61 (2017).

Methods

Animals. For experiments in wild-type animals, 4-month-old male CD-1 (ICR) mice (sexually experienced retired breeders; Charles River Laboratories) were used as subjects. Subjects were confirmed by Charles River Laboratories to have equal access, experience and success as breeders. For experiments in transgenic animals, C57BL/6J heterozygous orexin-Cre-IRES-GFP (gift from A. Yamanaka, see ref. [20]) or homozygous GAD2-Cre (Jackson Laboratory) mice were crossed to wild-type CD-1 mice, and the F_1 generation was used for experiments. This strategy was necessary to ensure a wide range of aggressive phenotypes in experimental animals, as C57BL/6J mice display relatively low levels of aggressive behavior[51]. At 3 months of age, F_1 transgenic male mice were paired with F_1 female mice for 2 weeks to gain sexual experience before being used for experiments. For experiments in transgenic mice, male littermates were randomly assigned to experimental groups. Eight-to-nine-week-old male C57BL/6J mice (20–30 g; Jackson Laboratory) were used as novel intruders. All mice were allowed 1 week of acclimation to the housing facilities before the start of experiments. Wild-type CD-1 and F_1 transgenic mice were singly housed, and C57BL/6J mice were housed in groups of five. All mice were maintained on a 12-h light:dark cycle (7:00 to 19:00) with ad libitum access to food and water. Consistent with many previous studies on aggression[31,49,52,53], behavioral experiments were conducted during the light phase. However, it is unclear whether our results are directly comparable to studies performed during the dark phase. Procedures were performed in accordance with the National Institutes of Health Guide for Care and approved by the Use of Laboratory Animals and the Icahn School of Medicine at Mount Sinai Institutional Animal Care and Use Committee. Additional information about mice used in this study can be found in the Life Sciences Reporting Summary.

Aggression screening/RI test. Aggression screening was performed as previously described by using the RI test[9]. After a minimum of 1 week of habituation to home cages, experimental mice were exposed to a novel C57BL/6J intruder for 5 min daily over three consecutive days. Each intruder presentation was performed in the home cage of the experimental mouse between 12:00 and 15:00 daily under white light conditions. During RI sessions, the cage top was removed to allow for unobstructed viewing and video recording of sessions. The duration and number of screening sessions were selected to prevent induction of stress- and anxiety-related behaviors in experimental CD-1 or F_1 hybrid mice[9]. All RI sessions were video recorded with a digital color video camera. Two blinded observers recorded (1) the latency to initial aggression and (2) the total duration of aggression. The initiation of aggression was defined by the first clear physical antagonistic interaction initiated by the resident mouse (usually a bite), not including grooming or pursuit behavior. Aggression was considered completed when the resident mouse had reoriented away from the intruder after the initiation of attack. This definition allows for slight breaks (less than 5 s) in continuous physical interaction within an aggressive bout, assuming the resident mouse has remained oriented toward the intruder throughout. Resident mice were defined as AGGs if they initiated aggression during all three screening sessions, whereas NONs were defined as those that showed no aggression during any screening session. Aggression screening was halted if an intruder showed any signs of injury in accordance with our previously published protocols[9,54].

Aggression CPP. We carried out the aggression CPP protocol according to Golden et al.[9]. Briefly, this task consisted of three phases: pre-test, acquisition (conditioning) and test. Mice were acclimated to the testing facility for 1 h before all testing. All phases were conducted under red light and sound-attenuated conditions. The CPP apparatus (Med Associates) consisted of two unique conditioning chambers with a neutral middle zone that allowed for unbiased entry into either conditioning chamber at the initiation of each trial. During the pre-test phase, mice were placed into the middle chamber of the conditioning apparatus and allowed to freely explore the apparatus for 20 min. There were no group differences in bias for either chamber, and conditioning groups were balanced in an unbiased fashion to account for pre-test preference. The acquisition phase consisted of three consecutive days with two conditioning trials each day for a total of six acquisition trials. Morning trials (between 8:00 and 10:00) and afternoon trials (between 15:00 and 17:00) consisted of experimental mice confined to one chamber for 10 min while in the presence or absence of a novel C57BL/6J intruder mouse. All groups were counterbalanced for the conditioning chamber. A total of three conditioning trials to the intruder-paired and intruder-unpaired context were performed. On the test day, experimental mice were placed into the middle arena without any intruders and allowed to freely explore the apparatus for 20 min. For optogenetic experiments, light was delivered during the full duration of the test phase only. Total locomotor activity was also recorded to ensure equal exploratory behavior between groups. Behavioral analysis of aggression CPP was performed by calculating (1) the raw CPP score (test phase duration in the paired chamber minus test phase duration in the unpaired chamber) and (2) the subtracted CPP score (test phase duration in the paired chamber subtracted from the pre-test phase duration in the paired chamber).

Open field test. The open field test was performed as previously described[55]. One week after the last RI, experimental mice were acclimated to the testing facility for 1 h before testing. Open field tests were performed in black plexiglass arenas (42 × 42 × 42 cm; Nationwide Plastics) under red light conditions. Testing sessions lasted for either 5 min (GAD2-specific OxR2 knockdown and systemic EMPA experiments) or 10 min (nonconditional OxR2 knockdown experiment). Behavior was tracked with Noldus Ethovision (Noldus) to record the total distance moved, time spent in the entire arena and time spent in the delineated 'center zone or 'corner zones' of the arena (24 × 24 cm).

Behavioral pharmacology. Mice were injected intraperitoneally with either 30 mg kg^{-1} EMPA (4558, Tocris) dissolved in 0.3% vol/vol Tween-80 in saline or vehicle (0.3% vol/vol Tween-80 in saline alone) 25 min before behavioral testing. For RI tests, animals were given EMPA 1 d and vehicle the other (counterbalanced for order, within-subjects design). For CPP and open field tests, half of the animals were given EMPA and half were given vehicle (between-subjects design).

Perfusion and brain tissue processing. For IHC and histologic analysis, mice were given a lethal dose of 15% chloral hydrate and transcardially perfused with cold PBS (pH 7.4) followed by fixation with cold 4% paraformaldehyde (PFA) in PBS. Brains were dissected and post-fixed for 24 h in 4% PFA. Coronal sections were prepared on a vibratome (Leica) at 50 µm to assess viral placement and perform IHC analysis.

For ISH, mice were rapidly decapitated and brains were removed and flash frozen in −30 °C isopentane for 30 s and then stored at −80 °C until sectioning. Coronal sections for in situ were prepared on a cryostat at 16-µm thickness and mounted directly on slides.

For RT–qPCR, mice were rapidly decapitated and the brains were extracted and placed in ice-cold PBS. Bilateral LHb 1-mm-diameter, 1-mm-thick tissue punches were taken and immediately flash frozen on dry ice and stored at −80 °C until RNA extraction.

RNA extraction, generation of cDNA and RT–qPCR. RNA was isolated from either brain tissue or N2A cells (American Type Culture Collection (ATCC)) using TRIzol (Invitrogen) and chloroform phase separation. The clear RNA layer was processed with the RNAeasy MicroKit (Qiagen) and analyzed with the NanoDrop (Thermo Fisher Scientific), and 500 ng of RNA was reverse transcribed to cDNA with qScript (95048-500, Quanta Biosciences). The resulting cDNA was diluted to 1 ng $µl^{-1}$.

For qPCR of hypocretin receptor 1 (*Hcrtr1*) and hypocretin receptor 2 (*Hcrtr2*), which encode the OxR1 and OxR2 proteins, 3 µl of cDNA was combined with 5 µl of Perfecta SYBR Green (95054-02 K, Quanta Biosciences), forward/reverse primers (1 µl total) and 1 µl of water. Samples were heated to 95 °C for 2 min followed by 40 cycles of 95 °C for 15 s, 60 °C for 33 s and 72 °C for 33 s. Analysis was performed using the $2^{-\Delta\Delta Ct}$ method. Samples were normalized to GAPDH. Primers used were as follows: GAPDH (F: AAC GGC ATT GTG GAA GG, R:GGA TGC AGG GAT GAT GTT CT), OxR1 (F: ATC CAC CCA CTG TTG TT, R: GGC CAG GTA GGT GAC AAT GA) and OxR2 (F: CAT CGT TGT CAT CTG GAT CG, R: GGC ACC AGA GTT TAC GGA AT).

For qPCR of all other transcripts, reactions were performed with 30 ng of cDNA per 10-ul reaction, Taqman Fast Advanced Master Mix (Life Technologies) and Taqman probes (Life Technologies) on a QuantStudio 7 Flex Real-Time PCR system (Life Technologies). Taqman probes used were: *Avpr2 (*Mm01193534_g1), *Drd1*(Mm02620146_s1), *Drd4* (Mm00432893_m1), *Glp1r* (Mm00445292_m1), *Htr3a* (Mm00442874_m1), *Mchr1* (Mm00653044_m1) and *Nmur* (Mm00515885_m1). Samples were held at 95 °C for 20 s and then cycled from 95 °C for 1 s to 60 °C for 20 s for 40 cycles. Gene expression was normalized to housekeeping genes *Abt1* (Mm00803824_m1) and *Hprt* (Mm03024075_m1) using the $2^{-\Delta\Delta Ct}$ method.

Generation and validation of AAV2 Cre-dependent OxR2 viral constructs. To create an effective Cre-dependent knockdown virus for OxR2, we used a micro-RNA (miR)-based approach. The miR was bicistronically expressed with IRES–eGFP for simple identification of infected cells. Briefly, we generated the OxR2 miR using the BLOCK-iT Pol II miR RNAi expression vector kit (Thermo Fisher Scientific). We used the shRNA sequence from our nonconditional OxR2 virus, which was previously validated to inhibit OxR2 expression[56]. A scrambled sequence was used as the control. We inserted the miR-containing oligonucleotides into a pcDNA6.2-GW-miR vector provided by the kit. The miR sequences, along with the 5′ and 3′ flanking regions, were then subcloned into a bicistronic IRES–GFP vector (pAAV-IRES-GFP, Cell Biolabs). This vector was nonconditional and can be expressed in mammalian cells. Suppression of OxR2 with the miR construct was validated in N2A cells (ATCC) by qPCR (see above). Once validated in vitro, the miR-IRES-GFP sequence was inserted into a Cre-dependent AAV2.Ef1a.DIO vector and packaged (Virovek) to produce AAV2-Ef1a-DIO-miROxR2-IRES-GFP-SV40pA and pAAV-Ef1a-DIO-miRscrambled-IRES-GFP-SV40pA. For overexpression of OxR2, we purchased a non-conditional DNA construct containing OxR2 (pcDNA-CMV-OxR2-Myc-FLAG-hGH-SV40, Genecopoeia) and verified overexpression in N2A cells using qPCR. To create an effective Cre-dependent overexpression virus for OxR2, the sequence for OxR2 was inserted into a Cre-dependent AAV2.Ef1a.DIO vector and packaged to produce AAV2-Ef1a-DIO-OxR2-SV40pA (Virovek). These AAVs were subsequently validated in vivo through injection into GAD2-Cre mice and ISH for GFP, GAD2 and OxR2.

IHC analysis, ISH and confocal microscopy. For IHC experiments, sections were incubated overnight in blocking solution (3% normal donkey serum, 0.3% Triton X-100 in PBS), washed three times in PBS for 10 min (30 min total) and then incubated for 24 h in primary antibodies diluted in blocking solution (goat anti-orexin-A (sc-8070, lot: J1818, 1:500 concentration, Santa Cruz Biotechnology) and chicken anti-GFP (GFP-1020, lot: 879848, 1:1,000 concentration, Aves Labs). According to manufacturers, goat polyclonal IgG anti-orexin-A antibody was validated in mouse and human tissue for immunofluorescence. This antibody was used in previous studies to detect orexin-A in mice using immunofluorescence[57]. According to manufacturers, chicken anti-GFP IgY was validated in transgenic mice expressing GFP using immunofluorescence. This antibody was used in previous publications to detect GFP in mice using immunofluorescence[58]. After primary antibody incubation, sections were then washed three times in PBS for 10 min (30 min total), incubated for 2 h in secondary antibodies diluted in blocking solution (donkey anti-goat Cy3 1:400 (705-165-003, Jackson ImmunoResearch) and donkey anti-chicken AlexaFluor 488 1:400 (703-545-155, Jackson ImmunoResearch) and washed three times in PBS for 10 min (30 min total). Finally, sections were counterstained with 1 µg ml^{-1} DAPI (Sigma) for 10 min and mounted on slides. Sections were allowed to dry on slides overnight, dehydrated with ethanol and then Citrisolv and cover-slipped with ProLong Diamond Antifade Mountant (P36970, Invitrogen). IHC analysis of orexin axons and GAD2 LHb cells was imaged using the AiryScan method on an LSM 880 confocal microscope (Carl Zeiss) and analyzed with Imaris (Bitplane). All other IHC analysis was imaged with an LSM 780 confocal microscope (Carl Zeiss) and analyzed with FIJI 1.0 (ImageJ) software.

For ISH experiments, we used the RNAScope Multiplex Fluorescent in situ kit (Advanced Cell Diagnostics) according to the manufacturer's instructions. Briefly, fresh-frozen sections were fixed in ice-cold 4% PFA in PBS for 15 min, serially dehydrated with EtOH (50%, 75% and 100%, each for 2 min) and pretreated with a protease (Protease IV, RNAScope) for 30 min. RNAscope probes (Advanced Cell Diagnostics) for eGFP (cat. 400281), GAD2 (cat. 415071), vGlut2 (cat. 319171) or OxR2 (cat. 460881) were hybridized at 40 °C for 2 h, serially amplified, counterstained with 1 µg ml^{-1} DAPI for 2 min and immediately cover-slipped with EcoMount mountant (Biocare Medical). ISH was imaged with a Zeiss LSM 780 confocal microscope at ×20, ×40 or ×63 magnification. mRNA puncta were quantified manually, blinded to experimental condition, using FIJI 1.0 software (ImageJ). Additional information about antibodies and ISH reagents can be found in the Life Sciences Reporting Summary.

In vitro electrophysiology. *Slice preparation.* Adult male mice were anesthetized with isoflurane and decapitated, and the brain was immediately removed and submerged into ice-cold sucrose-artificial CSF (aCSF) comprising (in mM) 233.7 sucrose, 26 $NaHCO_3$, 3 KCl, 8 $MgCl_2$, 0.5 $CaCl_2$, 20 glucose and 0.4 ascorbic acid. Coronal sections (350 µ thick) were sliced using a Leica VT1000S vibratome and allowed to equilibrate in recording aCSF (in mM: 117 NaCl, 4.7 KCl, 1.2 $MgSO_4$, 2.5 $CaCl_2$, 1.2 NaH_2PO_4, 24.9 $NaHCO_3$ and 11.5 glucose) oxygenated with 95% O_2/5% CO_2 for 1 h at room temperature. Slices were then transferred to the recording chamber where they were maintained at 31 °C and perfused (1.5 ml min^{-1}) with oxygenated aCSF.

Orexin bath application recordings. Two weeks before recording, GAD2-Cre was injected in the LHb (see coordinates in the next section) with AAV-hSyn-DIO-eYFP (UPenn Viral Core). Mice were then returned to their home cage to allow for viral expression before being killed for slice recordings. During recording, cells were identified as GAD2 positive by expression of eYFP in the LHb. Neurons were visualized on an upright epifluorescence microscope (BX50WI, Olympus) with a ×40 water-immersion objective and an infrared CCD monochrome video camera (Dage-MTI). Whole-cell recordings were performed with glass micropipettes (resistance, 2–4 MΩ) pulled from borosilicate glass capillaries using a P-87 micropipette puller (Sutter Instrument). The pipettes were filled with an intracellular solution containing 124 mm K-gluconate, 10 mm HEPES, 10 mm phosphocreatine di(Tris), 0.2 mm EGTA, 4 mm Mg_2ATP and 0.3 mm Na_2GTP, adjusted to an osmolarity of 280–290 mOsm and a pH of 7.3. Recordings were made with a Multiclamp 700B (Molecular Devices) in current clamp mode. Analog signals were low-pass filtered at 2 kHz and digitized at 5 kHz using a Digidata 1440 A interface and pClamp 10.0 software (Molecular Devices). Gigaseal and access to the intracellular neuronal compartment was achieved in voltage clamp mode, with the holding potential set at −70 mV. After rupturing the membrane, intracellular neuronal fluid equilibrated with the pipette solution without significant changes in series resistance or membrane capacitance. Cells were allowed to normalize for 5 min before recording. To test response of cells to orexin A (Phoenix Pharmaceuticals), we applied orexin A (1 µM) for 5 min in the circulating bath after a 2-min baseline period, followed by washout for 45–60 min. Orexin A was prepared freshly and dissolved in aCSF before being added to the recording bath.

Offline analysis was performed using Clampfit 10.0 (Molecular Devices). Spikes were counted during baseline, orexin wash-in and wash-out periods. To account for bath circulation, spikes were counted 2 min after the drug was added or after wash-out began. The Kruskal–Wallis test with Dunn's post hoc test for multiple comparisons was conducted to analyze the mean firing rate between groups (baseline, orexin wash-in and wash-out) using Prism 5 (GraphPad Software).

Slice optogenetic stimulation of LHb GAD2 neurons recording. Two weeks before recording, GAD2-Cre mice were injected with AAV1-DIO-ChR2-eYFP (UPenn Viral Core) in the LHb. Mice were then returned to their home cage to allow for viral expression before being killed for slice recordings. Recordings were obtained with borosilicate glass electrodes (resistance, 5–8 MΩ) filled with voltage clamp internal solution (in mM: 120 Cs-methanesulfonate, 10 HEPES, 10 Na-phosphocreatine, 8 NaCl, 5 TEA-Cl, 4 Mg-ATP, 1 QX-314, 0.5 EGTA and 0.4 Na-GTP). Cells were visualized on an upright DIC microscope equipped with a 460-nm objective-coupled LED (Prizmatix) for verification of ChR2 expression as well as optogenetic cellular manipulations. Data were low-pass filtered at 3 kHz and acquired at 10 kHz using Multiclamp 700B and pClamp 10.0 (Molecular Devices). The polarity of light-evoked stimulation (λ 460, 1 mW, 1–5 ms) of ChR2$^+$ terminals was determined by clamping cells at −70 mV (excitatory responses) and 0 mV (inhibitory responses). The monosynaptic nature of light-evoked currents was confirmed by bath application of tetrodotoxin (1 µM, Abcam) and 4-aminopyridine (100 µM, Abcam) as previously described[59,60]. The location of cells within the LHb was confirmed visually after recording.

Stereotaxic surgery and viral gene transfer. Mice were anesthetized with a mixture of ketamine (100 mg kg^{-1} body weight) and xylazine (10 mg kg^{-1} body weight) and placed securely in a stereotaxic frame (David Kopf Instruments). Next, 33-gauge syringes (Hamilton) were used to bilaterally infuse 0.5 µl of virus over 5 min, and virus was allowed to diffuse for 5 min before the needle was withdrawn. For LH injections, the coordinates from bregma were −1.3 mm AP, ± 1.1 mm ML and −5.1 mm DV at a 0° angle. For LHb injections, the coordinates from bregma were −1.7 mm AP, ± 0.6 mm ML and −2.7 mm DV at a 10° angle. For all optogenetics experiments, animals were implanted with an optical fiber at the same time as viral injection (−2.3 mm DV). Optic fibers (MFC_200/240-0.22_2.6mm_FLT, Doric Lenses) were secured to the skull using C&B Metabond adhesive luting cement (Parkell). For electrophysiology experiments, GAD2-Cre F_1 mice were injected bilaterally in the LHb with either AAV1-hSyn-DIO-eYFP or AAV1-hSyn-DIO-ChR2.eYFP (UPenn Viral Core). For orexin optogenetics experiments, AAV1-hSyn-DIO-NpHr3.0-eYFP, AAV1-hSyn-DIO-ChR2-eYFP or AAV1-hSyn-DIO-eYFP (UPenn Viral Core) was injected into the LH of orexin-Cre-IRES-GFP F_1 mice, and the optic fiber was placed in the LHb. Notably, IRES–GFP labeling of orexin neurons was not visible without enhancement of GFP signal using IHC, while viral eYFP was visible in perfused slices without amplification. This is evident in images of LH tissue from orexin-Cre animals injected with AAV-DIO-eYFP—only a portion of the total orexin neurons were green due to infection with the virus. The specificity of viral expression in orexin-positive neurons was confirmed (Fig. 5d and Supplementary Fig. 5). For GAD2 neuron optogenetics experiments, GAD2-Cre F_1 mice were injected bilaterally in the LHb with AAV1-hSyn.DIO-NpHr3.0-eYFP, AAV1-hSyn-DIO-ChR2-eYFP or AAV1-hSyn-DIO-eYFP (UPenn Viral Core). For conditional knockdown of OxR2, GAD2-Cre F_1 mice were injected bilaterally in the LHb with either AAV2-Ef1a-DIO-miROxR2-IRES-eGFP (knockdown) or AAV2-Ef1a-DIO-eGFP (generated for this study; Virovek). For conditional overexpression of OxR2, GAD2-Cre F_1 mice were injected bilaterally in the LHb with either AAV2-EF1a-DIO-GFP or AAV2-EF1a-DIO-OxR2. For nonconditional knockdown of OxR2 during optical stimulation of orexin terminals in the LHb, orexin-Cre F_1 mice were injected with AAV1-hSyn-DIO-ChR2 or AAV1-hSyn-DIO-eYFP in the LH and AAV2-hSyn-Cre plus AAV2-Ef1a-DIO-miR-OxR2-GFP or AAV2-Ef1a-DIO-miR-scrambled-GFP in the LHb. For fiber photometry in all LHb neurons, wild-type CD-1 mice were injected unilaterally in the LHb with AAV1-hSyn-GCaMP6s. For fiber photometry in GAD2 neurons, GAD2-Cre mice were injected unilaterally in the LHb with AAV9-hSyn-FLEX-GCaMP6s. Optic fibers for photometry (MFC_400/430-0.48_2.7mm_MF2.5-FLT, Doric Lenses) were implanted over the LHb at the same time as viral injection and secured with dental cement. AAV1 and AAV9 viruses were allowed 2–4 weeks for expression, whereas AAV2 viruses were allowed 4–6 weeks for expression.

Optogenetic stimulation. For blue light stimulation (ChR2), optical fibers (MFC_200/240-0.22_2.6mm_FLT, Doric Lenses) were connected to a 473-nm blue laser diode (BCL-473-050-M, Crystal Laser) using a patch cord with an FC/PC adapter (MFP_200/240/900-0.22_4m_FC-MF2.5, Doric Lenses). A function generator (33220A, Agilent Technologies) was used to generate 20-ms blue light pulses at 20 Hz. The intensity of light delivered to the brain was 7–10 mW. These parameters are consistent with previously validated and published protocols[9]. In particular, 20 Hz was selected for excitation of orexin neurons because in vitro experiments have demonstrated that 20 Hz stimulation is sufficient to elicit activation of orexin receptors[61].

For yellow light stimulation (NpHR), optical fibers were connected to a 561-nm yellow laser diode (CL561-050L, Crystal Laser) using an FC/PC adapter. A function generator (33220A, Agilent Technologies) was used to generate constant light pulses for 8 s followed by 2 s of light off. The intensity of the light

delivered to the brain was 7–10 mW. These parameters are consistent with previously validated and published protocols[9].

For all optogenetics experiments, experimental mice were habituated to patch cords for 5 d before testing in RI and aggression CPP. For RI experiments, mice were tested twice in the same day (in a counterbalanced fashion) in both laser-on and laser-off conditions with at least 4 h between sessions (within-subjects design). For CPP experiments, both groups (YFP or opsin) received laser stimulation (between-subjects design).

RT-PP. For RT-PP experiments, mice were placed in the center of an open field and allowed to freely explore for 20 min. The time spent on each side was recorded. For the first 10 min of testing, one side of the open field was paired with 20-ms pulses of 20 Hz blue light stimulation (473 nm, 7–10 mW intensity). For the second 10 min of testing, laser stimulation was paired with the opposite side of the open field. This was done to minimize inherent bias toward one side of the open field. An RT-PP score was calculated by subtracting the total time spent in the unstimulated side from the total time spent in the stimulated side.

Palatable food CPP. The palatable food CPP task consisted of three phases: pre-test, acquisition (conditioning) and test. Mice were acclimated to the testing facility for 1 h before all testing. All phases were conducted under red light conditions. The CPP apparatus (Med Associates) consisted of two unique conditioning chambers with a neutral middle zone that allowed for unbiased entry into either conditioning chamber at the initiation of each trial. During the pre-test phase, mice were placed into the middle chamber of the conditioning apparatus and allowed to freely explore the apparatus for 20 min. There were no group differences in bias for either chamber, and conditioning groups were balanced in an unbiased fashion to account for pre-test preference. The acquisition phase consisted of six consecutive days with two conditioning trials each day for a total of 12 acquisition trials. Morning trials (between 8:00 and 10:00) and afternoon trials (between 15:00 and 17:00) consisted of experimental mice confined to one chamber containing Reese's mini peanut butter cups for 20 min and one chamber containing standard chow for 20 min. Mice were exposed to Reese's mini peanut butter cups in the home cage before CPP testing to reduce effects of novelty during conditioning. All groups were counterbalanced for the conditioning chamber and conditioning time (a.m. versus p.m. pairings with peanut butter cups). On the test day, experimental mice were placed into the middle arena and allowed to freely explore the empty apparatus for 20 min. For optogenetic experiments, light was delivered during the full duration of the test phase only and not during conditioning. Behavioral analysis of CPP was performed by calculating (1) the raw CPP score (test phase duration in the paired chamber minus test phase duration in the unpaired chamber) and (2) the subtracted CPP score (test phase duration in the paired chamber subtracted by pre-test phase duration in the paired chamber).

Fiber photometry. *Apparatus: RI and aggression CPP.* A fiber optic patch cord (MFP_400/430/1100-0.37_3m_FC-MF2.5, Doric Lenses) was attached to the implanted fiber optic cannula with cubic zirconia sleeves. In turn, the fiber optic cable was coupled to the apparatus for light delivery and signal measurement. GCaMP6s signal was measured by passing 490-nm LED light (Thorlabs) through a GFP excitation filter (MF469, Thorlabs) and dichroic mirrors (DMLP425, MD498, Thorlabs) into the brain and focusing emitted light onto a photodetector (2151 femtowatt receiver, Newport) after passing it back through a dichroic mirror (MD498, Thorlabs), through a GFP emission filter (MF525-39, Thorlabs) and through a 0.50 N.A. microscope lens (62–561, Edmund Optics). To account for auto-fluorescence and possible motion artifacts during testing, a second 405-nm LED not corresponding to GCaMP6s delivered light through a violet excitation filter (FB405-10, Thorlabs) and the same dichroic mirrors as the 490-nm light. This signal was similarly directed into the brain and subsequently measured with the photodetector. Light at the fiber tip ranged from 30 to 75 µW but was constant across trials over days. Simultaneous recording of both 490- and 405-nm channels was achieved through sinusoidal modulation of the LEDs at different frequencies so that the signals could be easily unmixed. Signals were collected at a rate of 381 Hz and visualized using a real-time signal processor (RX8, Tucker-Davis Technologies) and PC OpenEx 2.20 software (Tucker-Davis Technologies).

Behavior: RI and aggression CPP. The timeline for aggression photometry experiments was as follows: viral injection and ferrule implantation (day 0), habituation to patch cord (days 14–15), RI recordings (days 16–18) and CPP recordings (days 21–25). Once hooked up to the apparatus, mice were allowed to rest for 10 min before the start of recording. Once recording was initiated, the GCaMP signal was allowed to stabilize for 2 min before the start of the behavioral trial. On each day of RI, we collected 5 min of baseline recordings followed by 5 min of intruder exposure. For CPP, photometry data were collected during the entire 20-min pre-test and test.

Analysis: RI and aggression CPP. Analysis of signals was done using custom-written MATLAB 8.5 code[36,62], which can be obtained from the authors upon reasonable request. The bulk fluorescent signal from each channel was normalized to compare across recording sessions and animals. Change in fluorescence was calculated as a percentage of the total fluorescence signal in the GCaMP channel (ΔF/F). The 405 channel served as the control channel and was subtracted from the GCaMP channel to eliminate signals due to auto-fluorescence, bleaching and the bending of the fiber optic cord during aggression. In general, these motion artifacts had very minimal effects on the overall GCaMP signal. Behavioral data were temporally aligned with fluorescence recording data by sending 1-s-interval TTL signals to the OpenEx software from Noldus Ethovision (Noldus) behavioral recording software. To identify peak signals, we first determined the median average deviation of the corrected/normalized datasets. Peak events that exceeded the median average deviation by 2.91 deviations were determined to be significant peaks, and this was in accordance with previous reports using the fiber photometry technique[36,62]. For analysis of LHb GCaMP activity during discrete behaviors in RI, average ΔF/F signals (%) in the 2 s before and after a discrete event (bite, approach, withdrawal) were compared. A bite was determined to occur at the moment of jaw closing on the body of the intruder; an approach was determined to occur at the moment of resident nose contact with any body part of the intruder; and a withdrawal was determined to occur at the moment body contact between resident and intruder ceased and one or both mice turned away from the site of interaction.

Apparatus: palatable food consumption. A branched fiber optic patch cord (BFP_200/230/900-0.37_FC-MF1.25, Doric Lenses) connected to the fiber photometry apparatus (Neurophotometrics) was attached to the implanted fiber optic cannula using a cubic zirconia sleeve. To record fluorescence signals from GCaMP6s, light from a 470-nm LED was band-pass filtered, collimated, reflected by a dichroic mirror and focused by a ×20 objective. LED light was delivered at a power that resulted in 75–150 uW of 470-nm light at the tip of the patch cord. Emitted GCaMP6s fluorescence was band-pass filtered and focused on the sensor of a CCD camera. To account for auto-fluorescence and possible motion artifacts during testing, a second 560-nm LED not corresponding to GCaMP6s delivered light through an excitation filter and the same dichroic mirrors as the 470-nm light. This signal was similarly directed into the brain and subsequently measured with the CCD camera. Simultaneous recording of both 470- and 560-nm channels was achieved through an integrated camera and image splitter (Flir Blackfly S series). Signals were collected at a rate of 40 Hz and visualized using the open-source software Bonsai 2.4 (http://bonsai-rx.org).

Behavior: palatable food consumption. All recordings were performed in the subjects' home cages between 10:00 and 12:00. The timeline for photometry experiments was as follows: viral injection and ferrule implantation (day 0), habituation to patch cord (days 14–15) and then recordings with food interactions (days 21–30). For food-restricted conditions, food was removed from cages at 17:00 the day before testing for a total food-restriction period of 18 h. Once attached to the patch cord, animals habituated for a period of 10 min while video and LED protocols were started. Baseline signal was taken from the final 5 min of recording before a 5-min exposure to food. Behaviors were scored manually using JWatcher 1.0 (Daniel T. Blumenstein, Janice C. Daniel and Christopher S. Evans, http://www.jwatcher.ucla.edu/).

Analysis: palatable food consumption. For fiber photometry analysis, the bulk fluorescent signal from each channel was normalized to compare across recording sessions and animals. Change in fluorescence was calculated as a percentage of the total fluorescence signal in the GCaMP channel (ΔF/F). The 560-nm channel was used to control for auto-fluorescence, bleaching and the bending of the fiber optic cord during testing. In general, these motion artifacts had very minimal effects on the overall GCaMP signal. For analysis of LHb GCaMP activity during food consumption, average ΔF/F signals in the 10 s before and after consumption were compared.

Statistics. All statistical details can be found in the figure legends, including type of statistical analysis used, *P* values, *n*, what *n* represents, degrees of freedom and *t* or *F* values. No statistical methods were used to predetermine sample sizes, but our sample sizes were similar to those reported in previous publications[8,9,44,63]. Animals and samples were assigned randomly to control and experimental groups, except for cases where aggressive behavior was compared between groups. In these cases, aggression was assessed and groups were counterbalanced for equal levels of aggression before manipulations were performed. Although experimenters were not blinded to group allocation for data collection, subsequent analysis of behavioral videos during the RI test was performed blinded to experimental conditions. Experimenters were blinded to experimental conditions for analysis of in situ hybridization. Data points were excluded if they were statistically significant outliers according to Grubb's test for outliers. This test was performed only once per dataset. In experiments requiring viral infection of a specific brain region, mice were excluded from behavioral analysis if the virus was found to be mis-targeted or not expressed according to predetermined anatomical criteria. No data were excluded for other reasons. For comparisons of two experimental groups, two-tailed paired (Student's, within-subject) or unpaired (between-subject) *t*-tests were used. For parametric datasets, comparisons of three or more groups were performed using one-way or two-way ANOVA tests followed by a Bonferroni post hoc test. For nonparametric datasets, comparisons of three or more groups were

performed using Kruskal–Wallis one-way ANOVA followed by Dunn's test for multiple comparisons. It was assessed whether groups displayed equal or unequal variances before using either parametric or nonparametric statistical tests. For all tests, $P < 0.05$ was deemed significant. Statistical analyses were performed using GraphPad Prism 5 software. Additional information about study design and statistics can be found in the Life Sciences Reporting Summary.

Reporting Summary. Further information on research design is available in the Nature Research Reporting Summary linked to this article.

Data availability

The data that support these findings are available from the corresponding author upon reasonable request.

Code availability

MATLAB code used to analyze photometry data is available from the corresponding author upon reasonable request.

References

51. Golden, S. A. et al. Persistent conditioned place preference to aggression experience in adult male sexually-experienced CD-1 mice. *Genes Brain Behav.* **16**, 44–55 (2017).
52. Couppis, M. H. & Kennedy, C. H. The rewarding effect of aggression is reduced by nucleus accumbens dopamine receptor antagonism in mice. *Psychopharmacology* **197**, 449–456 (2008).
53. Stagkourakis, S. et al. A neural network for intermale aggression to establish social hierarchy. *Nat. Neurosci.* **21**, 834–842 (2018).
54. Golden, S. A., Covington, H. E. 3rd, Berton, O. & Russo, S. J. A standardized protocol for repeated social defeat stress in mice. *Nat. Protoc.* **6**, 1183–1191 (2011).
55. Krishnan, V. et al. Molecular adaptations underlying susceptibility and resistance to social defeat in brain reward regions. *Cell* **131**, 391–404 (2007).
56. Arendt, D. H. et al. Anxiolytic function of the orexin 2/hypocretin A receptor in the basolateral amygdala. *Psychoneuroendocrinology* **40**, 17–26 (2014).
57. Whiddon, B. B. & Palmiter, R. D. Ablation of neurons expressing melanin-concentrating hormone (MCH) in adult mice improves glucose tolerance independent of MCH signaling. *J. Neurosci.* **33**, 2009–2016 (2013).
58. Daviaud, N., Friedel, R. H. & Zou, H. Vascularization and engraftment of transplanted human cerebral organoids in mouse cortex. *eNeuro* **5**, ENEURO.0219-18.2018 (2018).
59. Arruda-Carvalho, M. & Clem, R. L. Pathway-selective adjustment of prefrontal-amygdala transmission during fear encoding. *J. Neurosci.* **34**, 15601–15609 (2014).
60. Petreanu, L., Mao, T., Sternson, S. M. & Svoboda, K. The subcellular organization of neocortical excitatory connections. *Nature* **457**, 1142–1145 (2009).
61. Schöne, C. et al. Coreleased orexin and glutamate evoke nonredundant spike outputs and computations in histamine neurons. *Cell Rep.* **7**, 697–704 (2014).
62. Calipari, E. S. et al. In vivo imaging identifies temporal signature of D1 and D2 medium spiny neurons in cocaine reward. *Proc. Natl Acad. Sci. USA* **113**, 2726–2731 (2016).
63. Stagkourakis, S. et al. A neural network for intermale aggression to establish social hierarchy. *Nat. Neurosci.* **21**, 834–842 (2018).

Acknowledgements

The authors would like to thank S. Feng and C. Ferrer for their assistance with histology, N. Tzvaras for his assistance with microscopy and Virovek Inc. for cloning and packaging of AAV viruses. This work was supported by National Institutes of Health grants R01 MH114882-01 (to S.J.R.), R01 MH090264-06 (to S.J.R.), P50 MH096890 (to S.J.R.), P50 AT008661 (to S.J.R.), F31 MH111108-01A1 (to M.E.F.), T32 MH096678 (to M.E.F.), T32 MH087004 (to M.E.F.) and R01 MH51399 (to E.J.N.).

Author contributions

Stereotaxic surgeries were performed by M.E.F., H.A., M.L.P., S.A.G. and A.T. IHC analysis and ISH were performed by M.E.F., C.M. and K.B.L. Microscopy was performed by M.E.F. Molecular cloning of miR-OxR2 constructs was performed by H.A. qPCR was performed by K.L.C and M.E.F. Fiber photometry data collection was performed by M.E.F. and C.J.B., and fiber photometry analysis was performed by M.E.F., C.J.B., E.S.C., E.J.N. and S.B. OxR2 miRNA design was performed by R.J.D. Orexin-Cre mice were made by A.Y. Behavioral experiments were performed by M.E.F., H.A., L.L, C.J.B. and K.B.L. Electrophysiology experiments were performed by R.D.C, R.L.C., E.K.L., G.W.H. and B.M.A. Results were analyzed and interpreted by M.E.F. and S.J.R. The manuscript was written by M.E.F. and S.J.R. and edited by all authors.

Competing interests

S.J.R. and M.E.F. have a patent pending (US Patent Application 62/11,233) for the use of OxR2 antagonists to treat aggression.

Additional information

Supplementary information is available for this paper at https://doi.org/10.1038/s41593-020-0617-7.

Correspondence and requests for materials should be addressed to S.J.R.

Peer review information *Nature Neuroscience* thanks Stephen Mahler and the other, anonymous, reviewer(s) for their contribution to the peer review of this work.

Reprints and permissions information is available at www.nature.com/reprints.

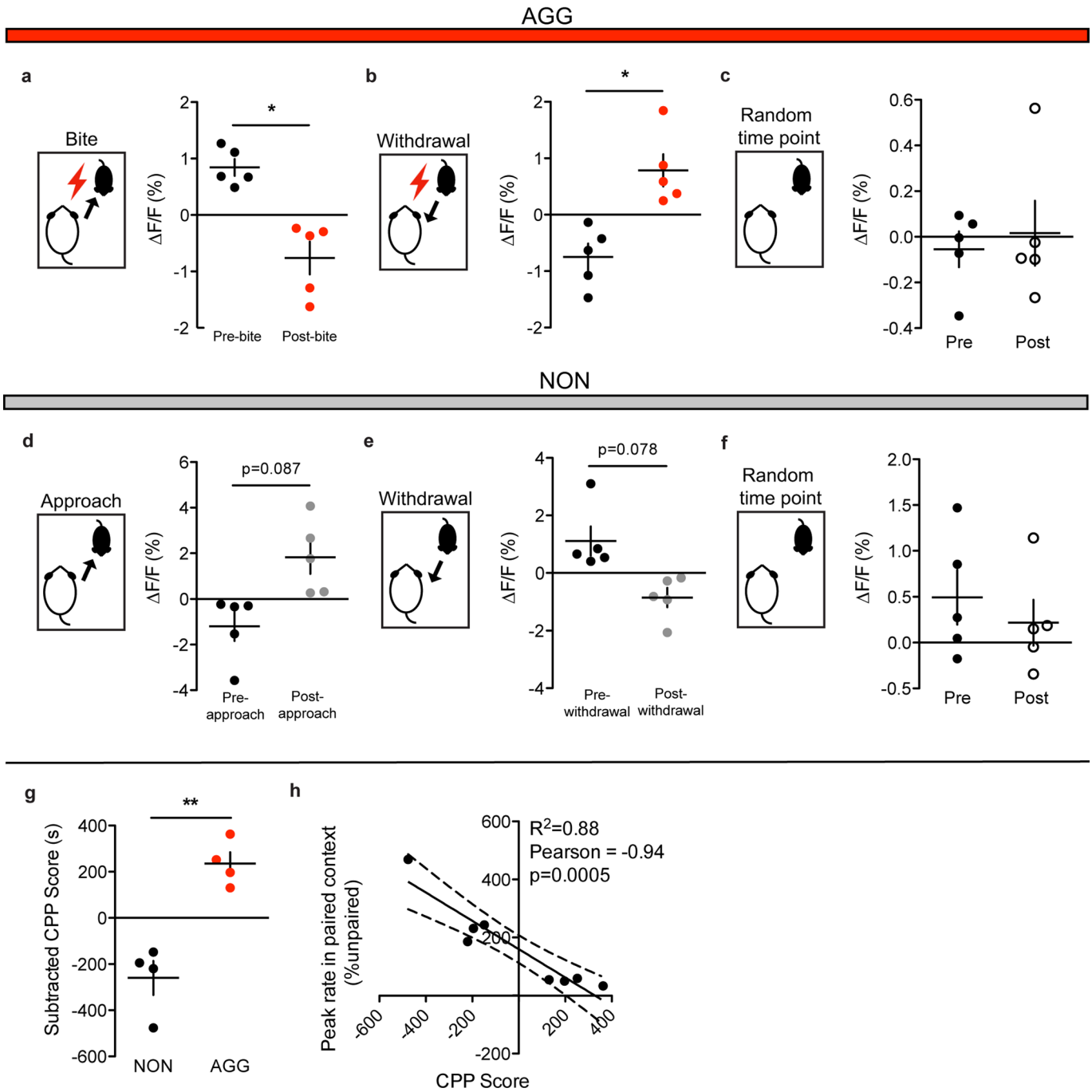

Extended Data Fig. 1 | LHb non-conditional fiber photometry supporting data. a, AGG average LHb activity was reduced following a bite on day 1 of RI (two-tailed paired t-test, n = 5 biologically independent mice, 3–5 bites per mouse, t(4)=3.763, p = 0.0197). **b**, AGG average LHb activity was increased following a withdrawal from aggression on day 1 of RI (two-tained paired t-test, n = 5 biologically mice, 3–5 withdrawals per mouse, t(4)=3.229, p = 0.03). **c**, AGG average LHb activity did not differ before and after random time points during RI on day 3 (two-tailed paired t-test, n = 5 biologically independent mice, t(4)=0.6545, p = 0.5485). **d**, NON average LHb activity was not significantly increased following intruder approach on day 1 of RI (two-tailed paired t-test, n = 5 biologically independent mice, 3-5 approaches per mouse, t(4)=2.25, p = 0.087). **e**, NON average LHb activity was not significantly reduced following withdrawal from social interactions on day 1 of RI (two-tailed paired t-test, n = 5 biologically independent mice, 3-5 withdrawals per mouse, t(4)=2.353, p = 0.078). **f**, NON average LHb activity did not differ before and after random time points during RI on day 3 (two-tailed paired t-test, n = 5 biologically independent mice, 5 time points per mouse, t(4)=0.553, p = 0.6221). **g**, AGGs used for fiber photometry experiments displayed significantly higher aggression CPP scores than NONs (two-tailed student's t-test, n = 4 biologically independent mice per group, t(6)=5.591, p = 0.0014). **h**, LHb peaks in the intruder paired context during the CPP preference test were negatively correlated with CPP score (two-tailed student's t-test, n = 8 biologically independent mice, Pearson correlation coefficient = -0.94, R^2 = 0.88, p = 0.0005). *p < 0.05, **p < 0.01. All data are expressed as mean ± SEM.

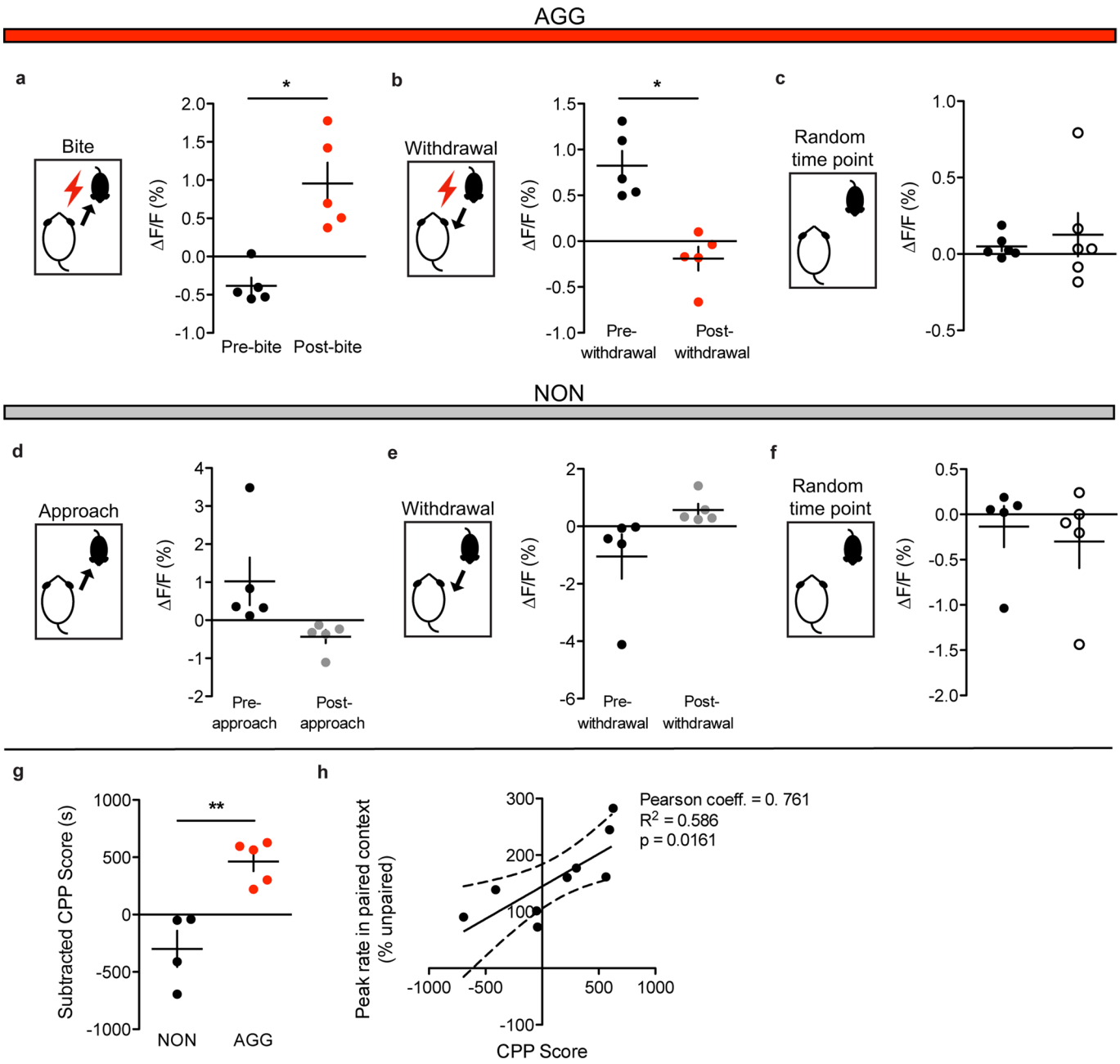

Extended Data Fig. 2 | LHB GAD2 neuron fiber phohometry supporting data. a, AGG LHb GAD2 neuron activity was increased following bites on day 1 of RI (two-tailed paired t-test, n = 5 biologically independent mice, 2-5 bites per mouse, t(4)=4.008, p = 0.016). **b**, AGG LHb GAD2 neuron activity was reduced following a withdrawal from an aggressive encounter on day 1 of RI (two-tailed paired t-test, n = 5 biologically independent mice, 3-5 withdrawals per mouse, t(4)=3.982, p = 0.0164). **c**, AGG LHb GAD2 neuron activity did not differ before and after random times points on day 3 of RI (two-tailed paired t-test, n = 5 biologically independent mice, 5 time points per mouse, t(4)=0.493, p = 0.6475). **d**, NON LHb GAD2 neuron activity was not different before and after an approach on day 1 of RI (two-tailed paired t-test, n = 5 biologically independent mice, 3-5 approaches per mouse, t(4)=1.843, p = 0.1406). **e**, NON LHb GAD2 neuron activity was not different before and after a withdrawal from a non-aggressive social interaction on day 1 of RI (two-tailed paired t-test, n = 5 biologically independent mice, 3-5 withdrawals per mouse, t(4)-1.633, p = 0.1777). **f**, NON LHb GAD2 neuron activity did not differ before and after random time points on day 3 of RI (two-tailed paired t-test, n = 5 biologically independent mice, t(4)=1.721, p = 0.1634). **g**, GAD2-cre AGGs used for fiber photometry experiments displayed significantly higher aggression CPP scores than GAD2-cre NONs (two-tailed paired t-test, n = 5 biologically independent mice, t(4)=2.885, p = 0.0448). **h**, LHb GAD2 neurons peaks in the intruder paired context during the CPP preference test were positively correlated with CPP score (two-tailed student's t-test,A n = 10 biologically independent mice, Pearson correlation coefficient = 0.761 m, $R^2 = 0.586$, p = 0.0161). *p < 0.05, **p < 0.01. *p < 0.05. All data are expressed as mean ± SEM.

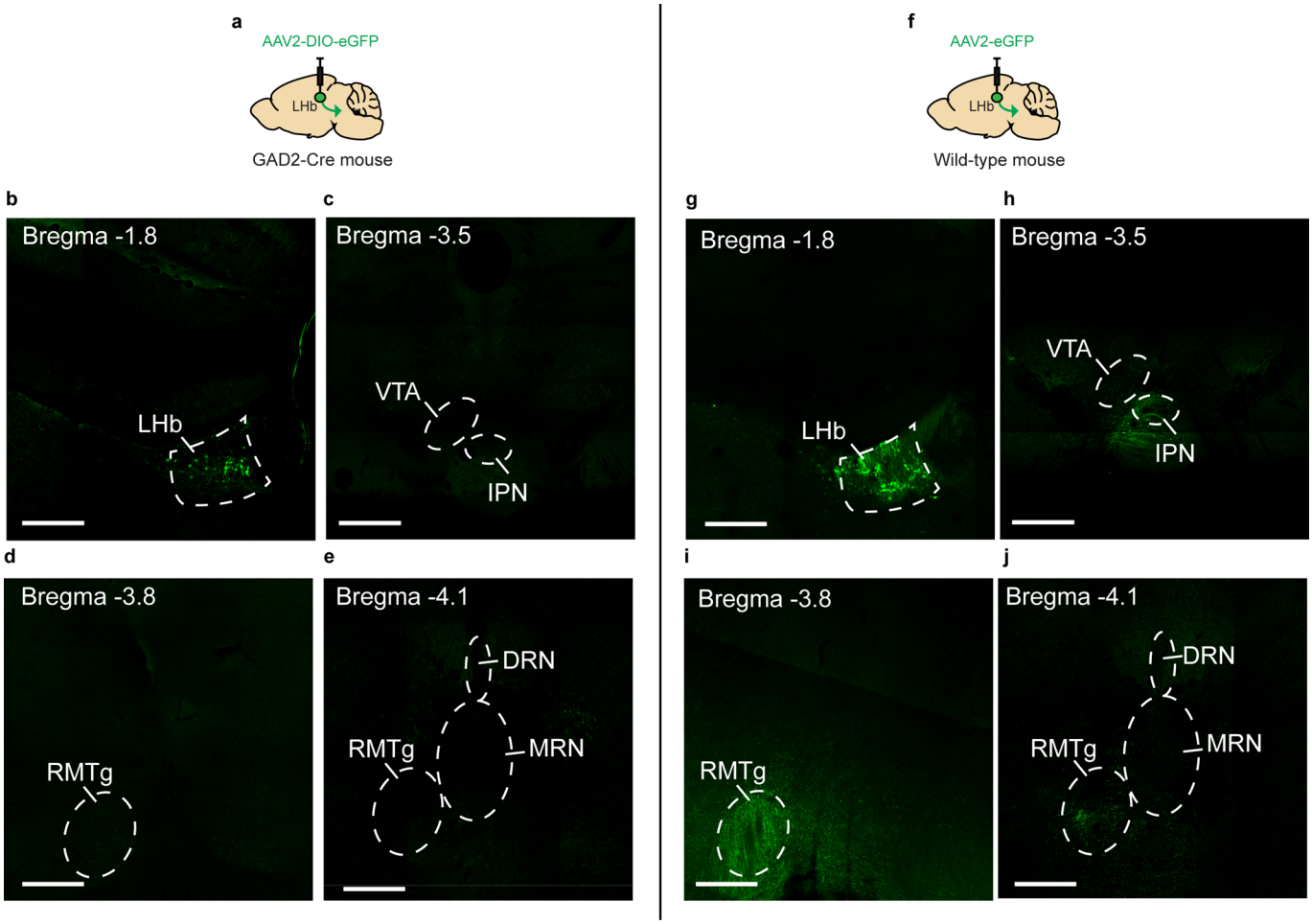

Extended Data Fig. 3 | Anterograde tracing of LHB GAD2 neuron projections. a, Schematic of surgical manipulations for anterograde tracing of GAD2 LHb neurons. **b**, Representative image of viral infection in GAD2 LHb neurons. Experimental images were obtained from 3 biologically independent mice, three slices per mouse, with similar results obtained. **c**, Representative image of the interpeduncular nucleus (IPN) and ventral tegmental area (VTA) in mice expressing eGFP in GAD2 LHb neurons. Experimental images were obtained from 3 biologically independent mice, three slices per mouse, with similar results obtained. **d**, Representative image of the rostromedial tegmental nucleus (RMTg) in mice expressing eGFP in GAD2 LHb neurons. Experimental images were obtained from 3 biologically independent mice, three slices per mouse, with similar results obtained. **e**, Representative image of the RMTg and anterior dorsal and median raphe nuclei (DRN and MRN) in mice expressing eGFP in GAD2 LHb neurons. Experimental images were obtained from 3 biologically independent mice, three slices per mouse, with similar results obtained. **f**, Schematic of surgical manipulations for non-conditional anterograde tracing of LHb neurons. **g**, Representative image of viral infection in LHb neurons. Experimental images were obtained from 3 biologically independent mice, three slices per mouse, with similar results obtained. **h**, Representative image of the interpeduncular nucleus (IPN) and ventral tegmental area (VTA) in mice expressing eGFP in LHb neurons. Experimental images were obtained from 3 biologically independent mice, three slices per mouse, with similar results obtained. **i**, Representative image of the rostromedial tegmental nucleus (RMTg) in mice expressing eGFP in LHb neurons. Experimental images were obtained from 3 biologically independent mice, three slices per mouse, with similar results obtained. **j**, Representative image of the RMTg and anterior dorsal and median raphe nuclei (DRN and MRN) in mice expressing eGFP in LHb neurons. Experimental images were obtained from 3 biologically independent mice, three slices per mouse, with similar results obtained. Scale bars= 500 μm.

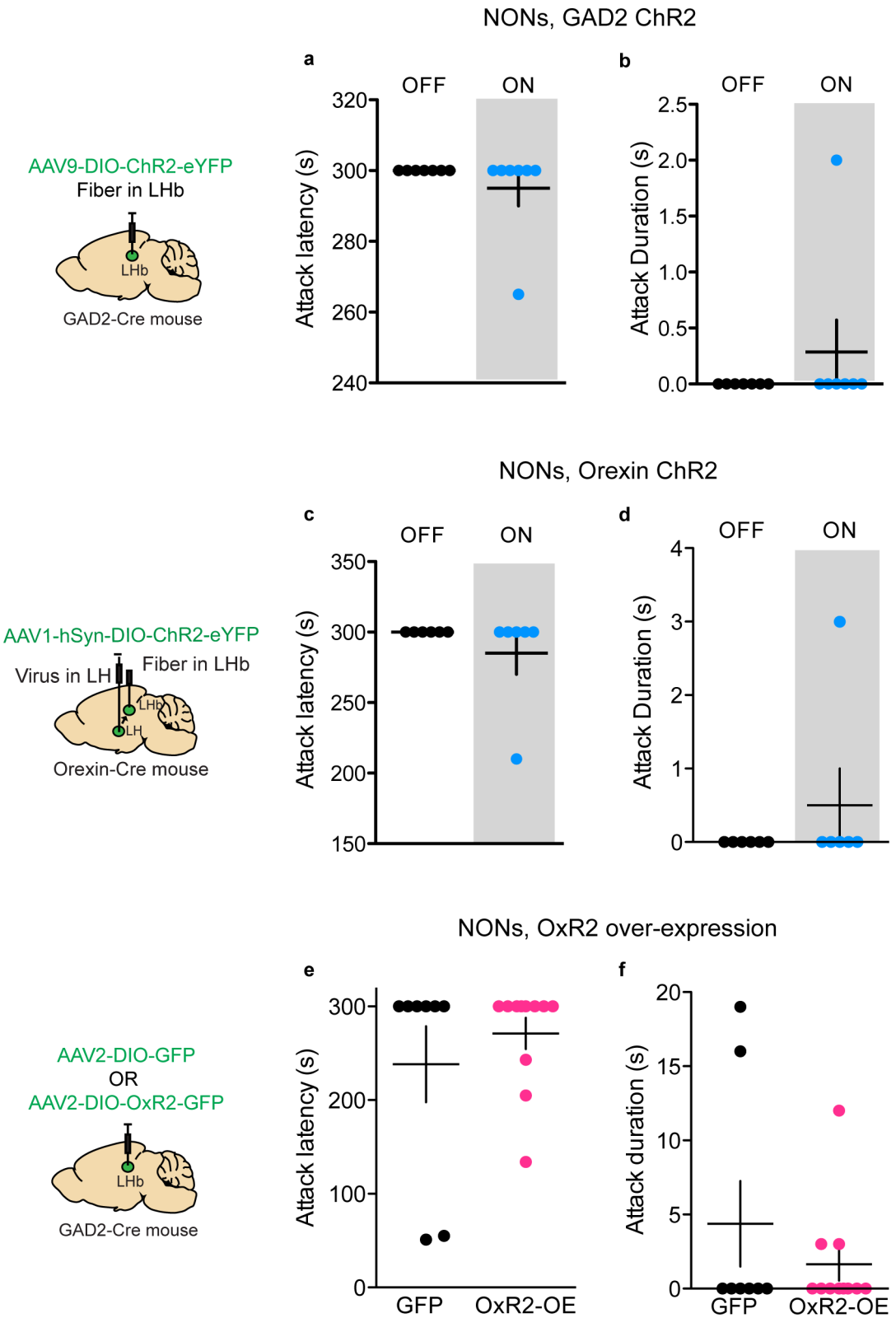

Extended Data Fig. 4 | RI behavior in NONs during optogenetic stimulation of OxR2 over-expression in LHb GAD2 neurons. a, ChR2-mediated stimulation of GAD2 LHb neurons in NONs did not affect attack latency during RI (two-tailed paired t-test, n = 7 biologically independent mice, t(6)=1.0, p = 0.3559). **b**, ChR2-mediated stimulation of GAD2 LHb neurons in NONs did not affect attack duration during RI (two-tailed paired t-test, n = 7 biologically independent mice, t(6)=1.0, p = 0.3559). **c**, ChR2-mediated stimulation of orexin terminals in the LHb did not affect attack latency during RI (two-tailed paired t-test, n = 6 biologically independent mice, t(5)=1.0, p = 0.3632). **d**, ChR2-mediated stimulation of orexin terminals in the LHb did not affect attack duration during RI (two-tailed paired t-test, n = 5 biologically independent mice, t(5)=1.0, p = 0.3632). **e**, Over-expression of OxR2 in GAD2 LHb neurons in NONs did not affect attack latency during RI (two-tailed student's t-test, n = 8 biologically independent GFP mice and n = 11 biologically independent OxR2-OE mice, t(17)=0.8338, p = 0.4160). **f**, Over-expression of OxR2 in GAD2 LHb neurons in NONs did not affect attack duration during RI (two-tailed student's t-test, n = 8 biologically independent GFP mice and n = 11 biologically independent OxR2-OE mice, t(17)=0.9951. All data are expressed as mean ± SEM.

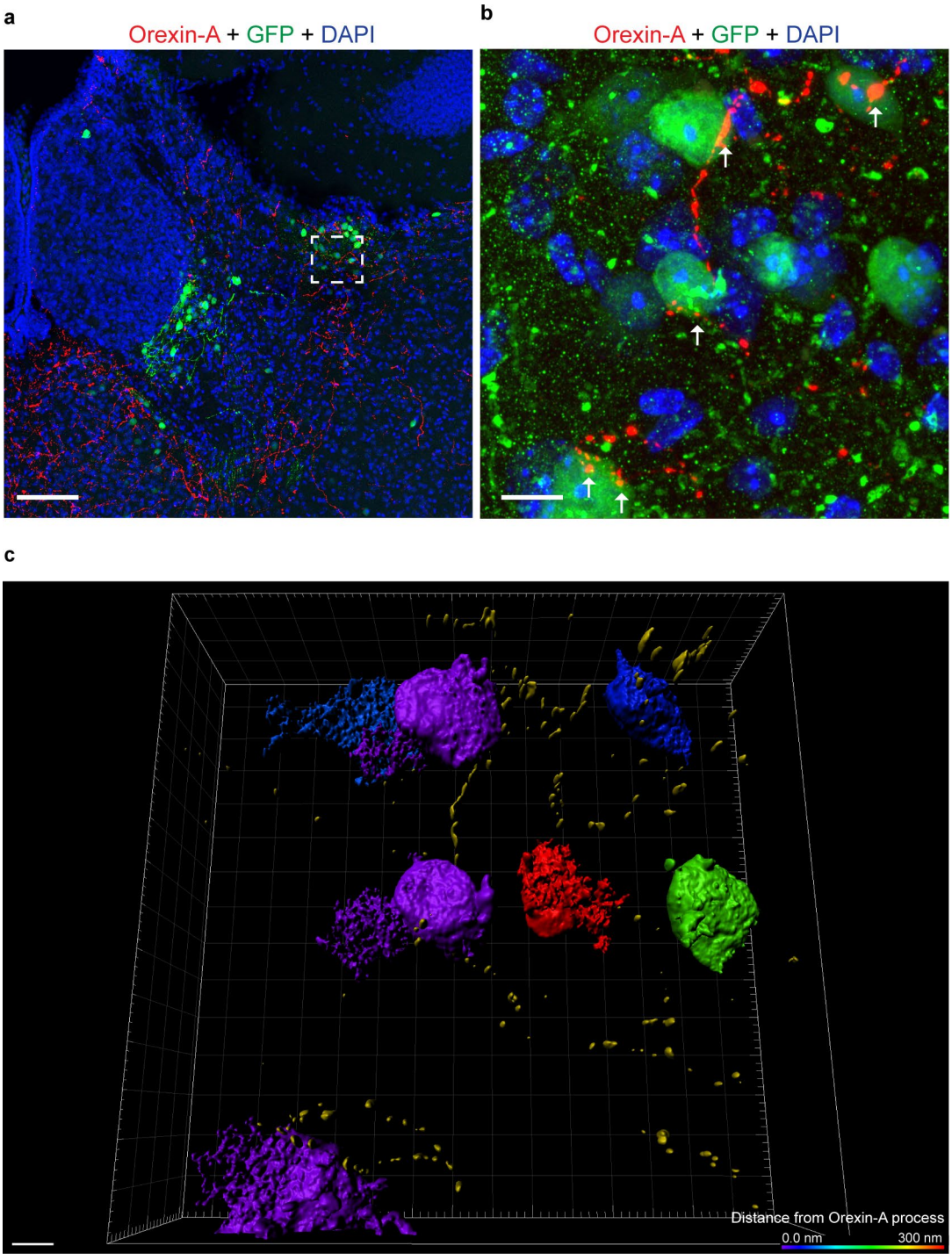

Extended Data Fig. 5 | Histology and 3D rendering of LHb GAD2 neurons and orexin axons. a, Immunohistochemistry for orexin-A (red), DAPI (blue), and eGFP (green) in a GAD2-Cre mouse injected with AAV-DIO-eGFP, scale bar = 300 μm. Experimental images were taken from 3 biologically independent mice, 3 slices per mouse, with similar results obtained. **b**, Immunohistochemistry for orexin-A (red), DAPI (blue), and GFP (green) in a GAD2-Cre mouse injected with AAV-DIO-eGFP, scale bar = 10 μm. Experimental images were taken from 3 biologically independent mice, 3 slices per mouse, with similar results obtained. **c**, 3D rendering of image in b, color of GAD2 neuron coincides with estimated distance from orexin-A axon according to key in lower right corner, scale bar = 5 μm. Experimental images were taken from 3 biologically independent mice, 3 slices per mouse, with similar results obtained.

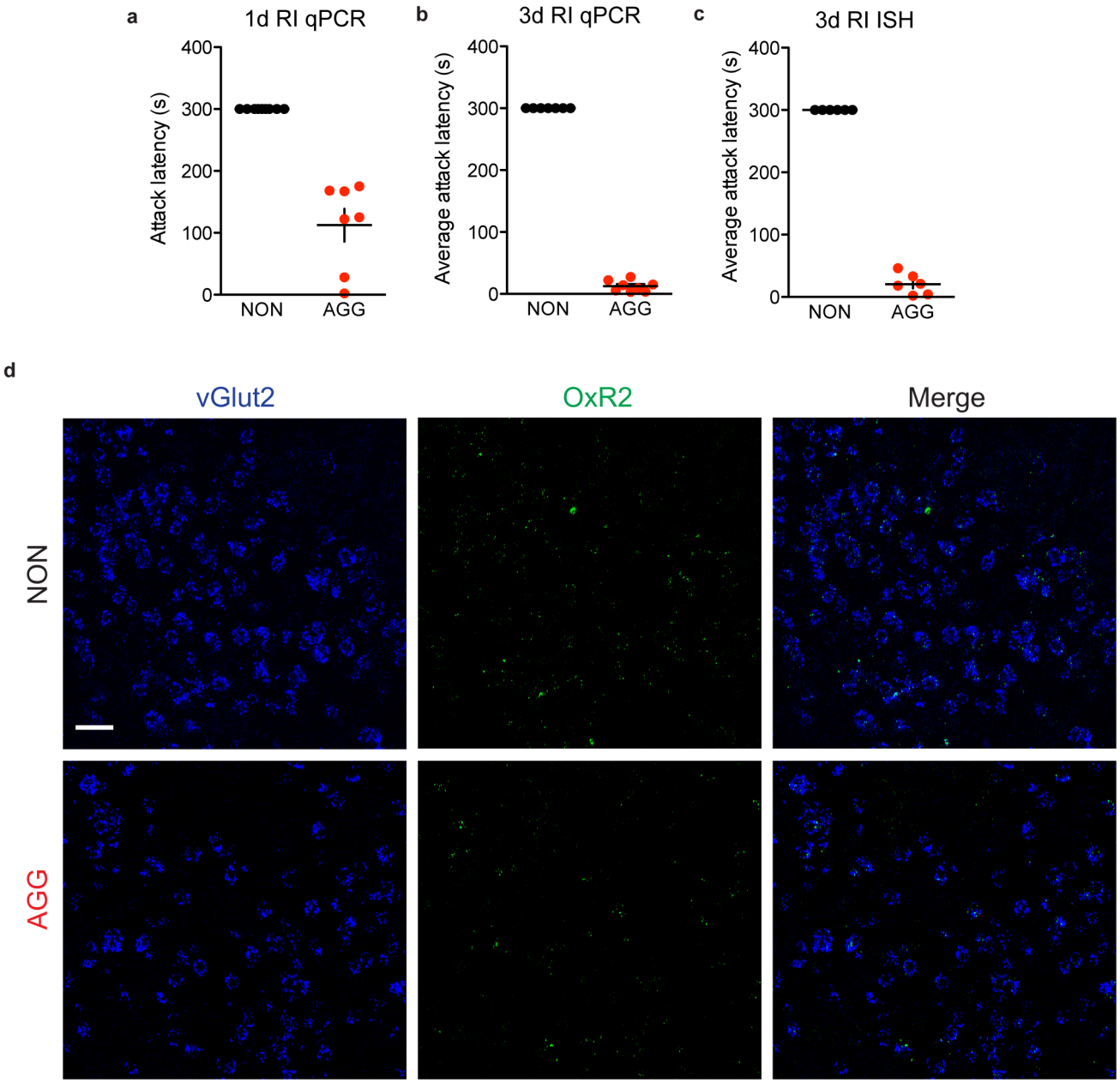

Extended Data Fig. 6 | Attack latencies for AGGs and NONs used in qPCR and ISH experiments. a, Attack latency for one day of RI in mice used for LHb qPCR, n = 9 biologically independent NON mice, n = 7 biologically independent AGG mice. **b**, Average attack latency for three days of RI in mice used for LHb qPCR, n = 7 biologically independent NON mice, n = 8 biologially independent AGG mice. **c**, Average attack latency for three days of RI in mice used for LHb OxR2 ISH, n = 6 biologically independent NON mice, n = 6 biologically independent AGG mice. **d**, Representative images from OxR2 ISH in AGG and NON LHb vGlut2 neurons following RI, accompanies Fig. 5j, scale bar = 20 μm. Notably, OxR2 expression was barely detectable in these neurons in AGGs or NONs, which is in line with our findings showing low OxR2 expression in vGlut2 neurons in Fig. 5b, c. Experimental images were taken from 12 biologically independent mice, 2 slices per mouse, with similar results obtained. All data are expressed as mean ± SEM.

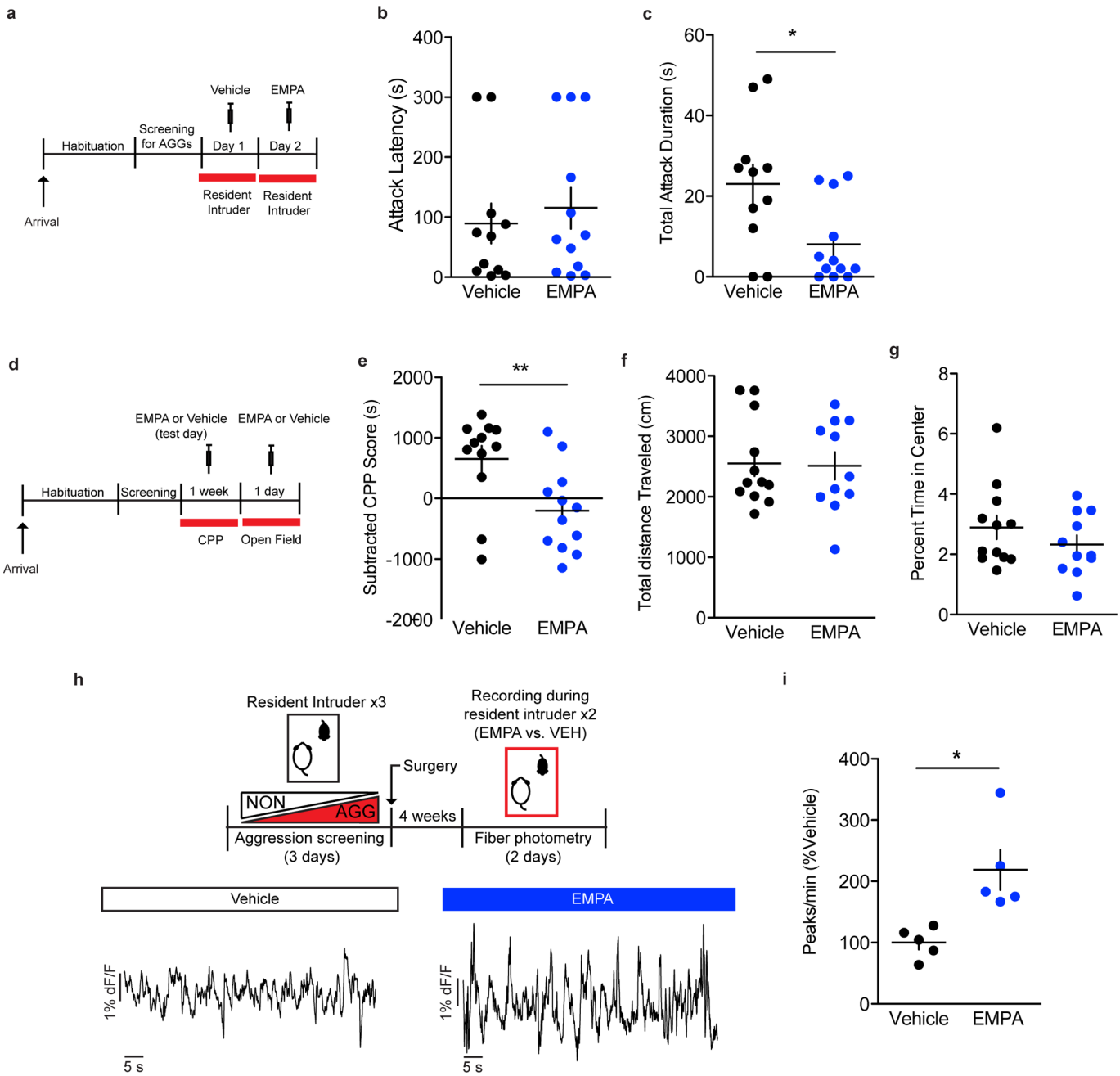

Extended Data Fig. 7 | Effects of systemic antagonism of OxR2 with EMPA on aggression and LHb activity. a, Experimental scheme for OxR2 systemic antagonism RI experiment. **b**, RI test attack latency in animals treated with EMPA and vehicle (two-tailed paired t-test, n = 11 biologically independent mice per group, t(10)=0.3215, p = 0.758). **c**, RI test attack duration in animals treated with EMPA and vehicle (two-tailed paired t-test, n = 11 biologically independent mice per group, t(10)=2.888, p = 0.016).**d**, Experimental scheme for OxR2 systemic antagonism aggression CPP and locomotion experiments. **e**, Aggression CPP for animals treated with EMPA and vehicle (two-tailed student's t-test, n = 12 biologically independent vehicle mice and n = 11 biologically independent EMPA mice, t(21)=2.885, p = 0.0086). **f**, Locomotor activity in the open field for animals treated with EMPA and vehicle (two-tailed student's t-test, n = 12 biologically independent vehicle mice and n = 11 biologically independent EMPA mice, t(21)=0.1301, p = 0.8991). **g**, Anxiety-related behavior in the open field for animals treated with EMPA or vehicle (two-tailed student's t-test, n = 11 biologically independent mice per group, t(21)=1.134, p = 0.2695) **h**, Representative fiber photometry traces in an animal treated with vehicle and EMPA. **i**, LHb GCaMP peaks during RI during vehicle and EMPA treatment (two-tailed paired t-test, n = 5 biologically independent mice, t(4)=2.946, p = 0.0421). *p < 0.05, **p < 0.01. All data are expressed as mean ± SEM.

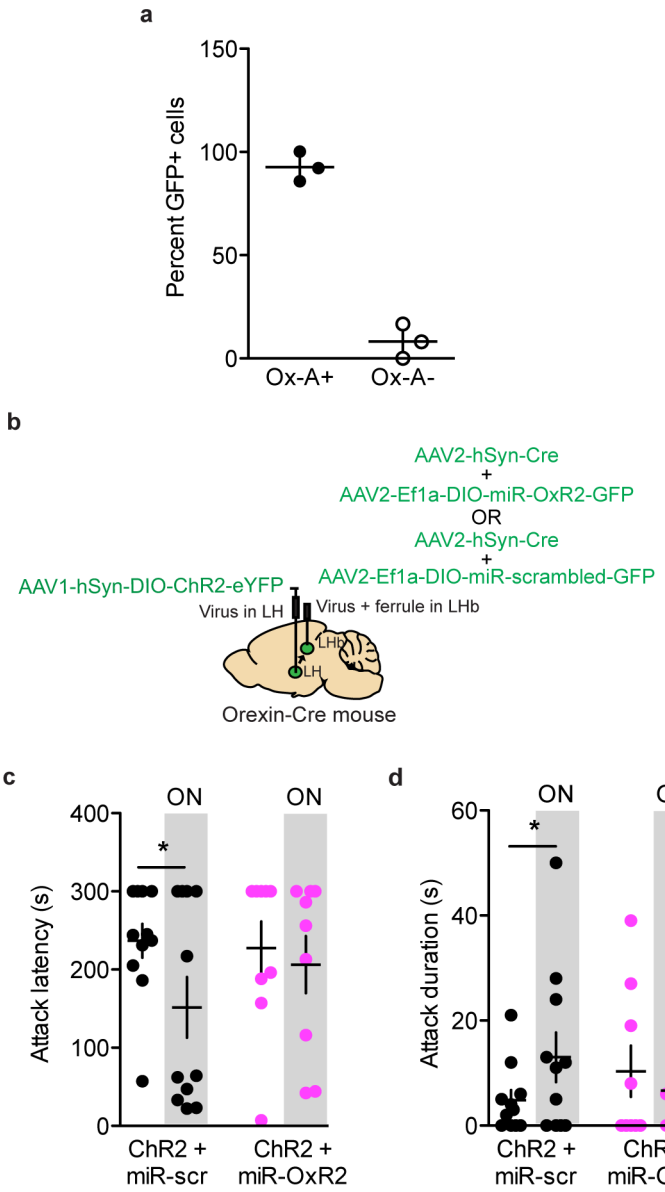

Extended Data Fig. 8 | LHb orexin-ChR2 experiments supporting data. a, >90% of neurons infected with AAV1-DIO-YFP were positive for orexin-A protein as determined by immunohistochemistry, n = 3 biologically independent mice, 3 slices per mouse. **b**, Surgical manipulations for ChR2-mediated activation of orexin terminals in the LHb with concurrent knockdown of LHb OxR2. **c**, Optogenetic stimulation of orexin terminals in the LHb reduced attack latency in mice treated with the miR-scrambled virus, but not the miR-OxR2 virus (two-tailed paired t-test, miR-scrambled: n = 11 biologically independent mice, $t(10)=2.424$, $p = 0.0358$; miR-OxR2: n = 9 biologically independent mice, $t(8)=0.5281$, $p = 0.6117$). **d**, Optogenetic stimulation of orexin terminals in the LHb increased attack duration in mice treated with the miR-scrambled virus, but not the miR-OxR2 virus (two-tailed paired t-test, miR-scrambled: n = 11 biologically independent mice, $t(10)=2.260$, $p = 0.0474$; miR-OxR2: n = 9 biologically independent mice, $t(8)=0.8493$, $p = 0.4204$). *$p < 0.05$. All data are expressed as mean ± SEM.

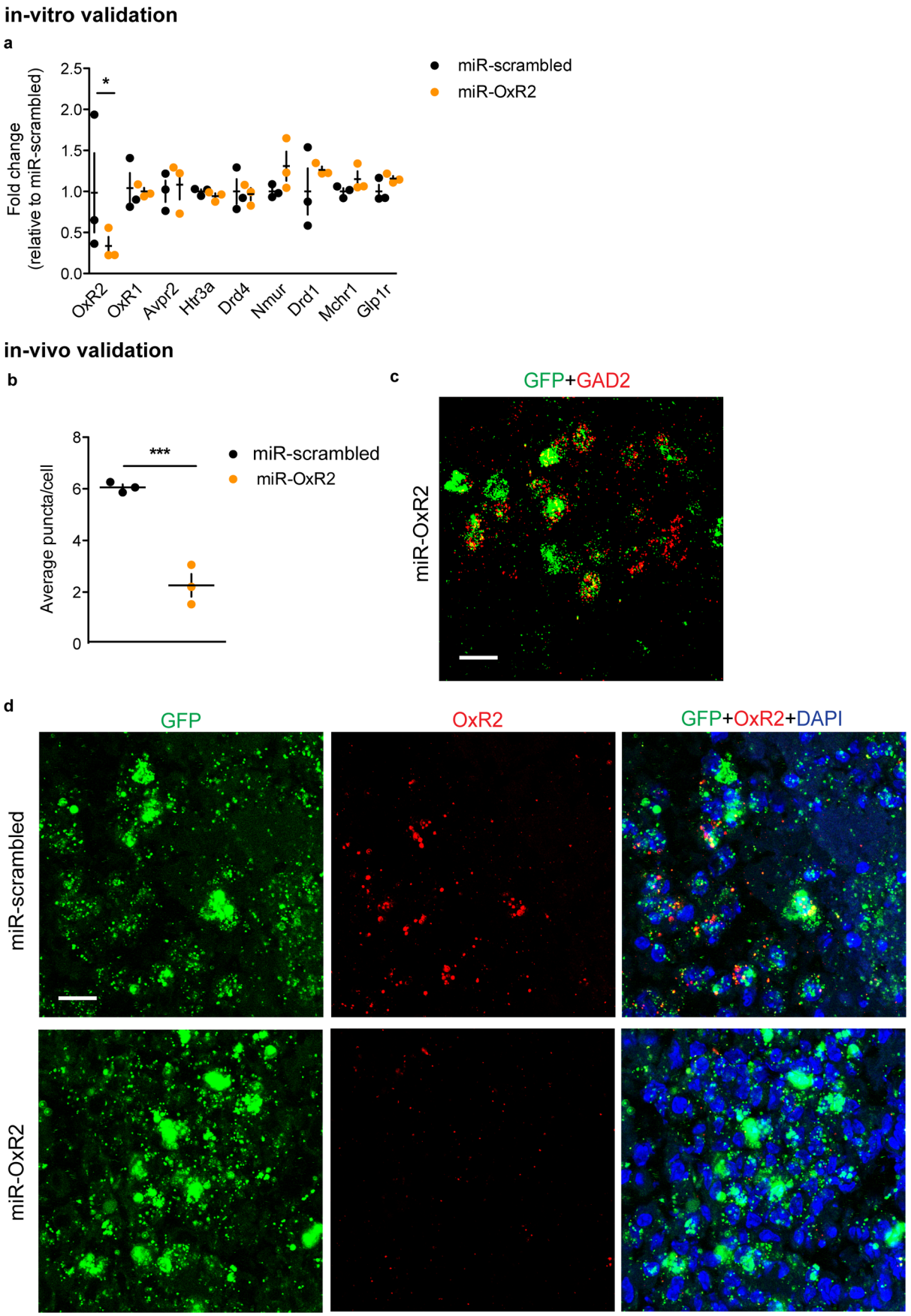

Extended Data Fig. 9 | See next page for caption.

Extended Data Fig. 9 | *In-vitro* and *in-vivo* validation of AAV-DIO-miR-OxR2 virus. a, N2A cells treated with miR-OxR2 construct selectively reduced OxR2 expression compared to cells treated with miR-scrambled construct, but did not reduce expression of related transcripts (two-tailed student's t-test, n = 3 biologically independent plates per group, 3 replicates per plate; OxR2: t(4)=2.402, p = 0.0482; OxR1: t(4)=0.2123, p = 0.8423; Avpr2: t(4)=0.3686, p = 0.7311; Htr3a: t(4)=1.309, p = 0.2607; Drd4: t(4)=0.1925, p = 0.8567; Nmur: t(4)=1.672, p = 0.1699; Drd1: t(4)=0.9239, p = 0.4078; Mchr1: t(4)=1.467, p = 0.2163; Glpr1: t(4)=1.785, p = 0.1488). **b**, GAD2-Cre mice injected with AAV-DIO-miR-OxR2 displayed reduced expression of OxR2 compared to mice injected with AAV-DIO-miR-scrambled as determined by ISH (two-tailed student's t-test, n = 3 mice, 2 slices per mouse, t(4)=18.44, p = 0.0001). **c**, Representative image of GFP expression localized to GAD2 LHb neurons in GAD2-Cre mice injected with AAV-DIO-miR-OxR2, scale bar = 25 μm. Experimental images were obtained from 6 biologically independent mice, 2 slices per mouse, with similar results obtained. **d**, Representative images of OxR2 expression in GAD2 LHb neurons infected with AAV-DIO-miR-OxR2 or AAV-DIO-miR-scrambled, scale bar, 20 μm. *p < 0.05, ***p < 0.001. All data are expressed as mean ± SEM.

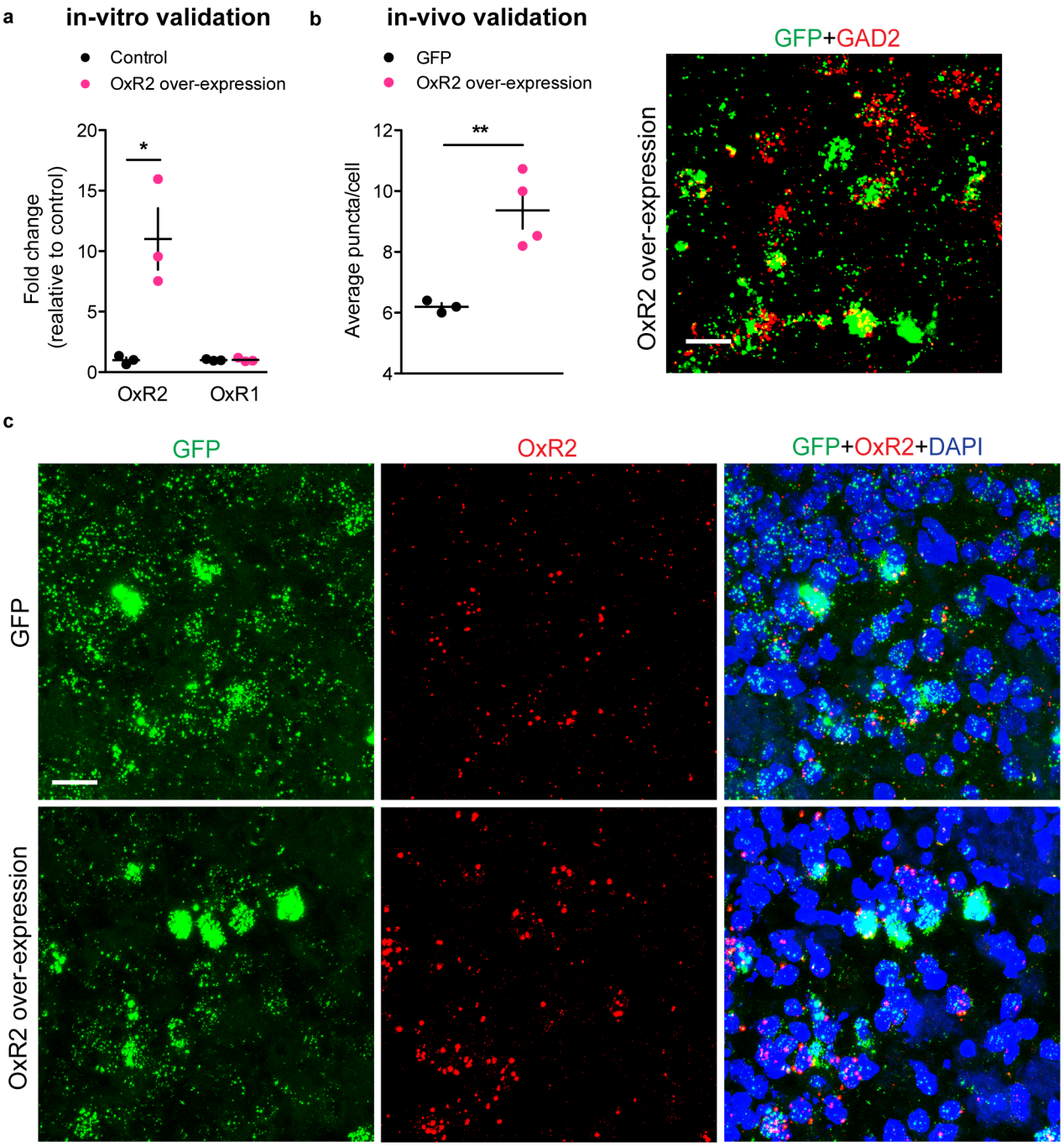

Extended Data Fig. 10 | *In-vitro* and *in-vivo* validation of AAV-DIO-OxR2 over-expression virus. a, N2A cells treated with OxR2 over-expression construct selectively increased OxR2 expression compared to controls (two-tailed student's t-test, n = 3 biologically independent plates per group, 3 replicates per plate, OxR2: t(4)=3.939, p = 0.0171; OxR1: t(4)=0.1238, p = 0.9075). **b**, GAD2-Cre mice injected with AAV-DIO-OxR2 displayed increased expression of OxR2 compared to mice injected with AAV-DIO-GFP as determined by ISH (two-tailed student's t-test, n = 3 biologically independent mice, 2 slices per mouse, t(4)=4.417, p = 0.0069) (left). Representative image of GFP expression localized to GAD2 LHb neurons in GAD2-Cre mice injected with AAV-DIO-OxR2, scale bar = 25 μm (right). Experimental images were obtained from 7 biologically independent mice, 2 slices per mouse, with similar results obtained. **c**, Representative images of OxR2 expression in GAD2 LHb neurons infected with AAV-DIO-OxR2 or AAV-DIO-GFP, scale bar = 25 μm. *p < 0.05, **p < 0.01. Experimental images were taken from 7 biologically independent mice, 2 slices per mouse, with similar results obtained. All data are expressed as mean ± SEM.

nature research

Corresponding author(s): Scott J. Russo

Last updated by author(s): Feb 20, 2020

Reporting Summary

Nature Research wishes to improve the reproducibility of the work that we publish. This form provides structure for consistency and transparency in reporting. For further information on Nature Research policies, see Authors & Referees and the Editorial Policy Checklist.

Statistics

For all statistical analyses, confirm that the following items are present in the figure legend, table legend, main text, or Methods section.

n/a	Confirmed	
☐	☒	The exact sample size (*n*) for each experimental group/condition, given as a discrete number and unit of measurement
☐	☒	A statement on whether measurements were taken from distinct samples or whether the same sample was measured repeatedly
☐	☒	The statistical test(s) used AND whether they are one- or two-sided *Only common tests should be described solely by name; describe more complex techniques in the Methods section.*
☒	☐	A description of all covariates tested
☐	☒	A description of any assumptions or corrections, such as tests of normality and adjustment for multiple comparisons
☐	☒	A full description of the statistical parameters including central tendency (e.g. means) or other basic estimates (e.g. regression coefficient) AND variation (e.g. standard deviation) or associated estimates of uncertainty (e.g. confidence intervals)
☐	☒	For null hypothesis testing, the test statistic (e.g. *F*, *t*, *r*) with confidence intervals, effect sizes, degrees of freedom and *P* value noted *Give P values as exact values whenever suitable.*
☒	☐	For Bayesian analysis, information on the choice of priors and Markov chain Monte Carlo settings
☒	☐	For hierarchical and complex designs, identification of the appropriate level for tests and full reporting of outcomes
☐	☒	Estimates of effect sizes (e.g. Cohen's *d*, Pearson's *r*), indicating how they were calculated

Our web collection on statistics for biologists contains articles on many of the points above.

Software and code

Policy information about availability of computer code

Data collection	Behavioral experiments were assayed automatically using the video tracking software Ethovision XT 11 (Noldus). Acquisition of electrophysiological data was performed with pClamp 10.0 (Molecular Devices). Fiber photometry data for aggression studies was acquired with open source OpenEx software 2.20 controlling an RX8 lock-in amplifier (Tucker-Davis Technologies). Fiber photometry for food studies was acquired with open source Bonsai software 2.4.0 and custom Neurophotometrics (Neurophotometrics, Ltd) hardware.
Data analysis	Analysis of electrophysiological data was performed with Clampfit 10.0 (Molecular Devices). Analysis of fiber photometry data was performed with Matlab 8.5 (Mathworks, Inc.). Histological data was analyzed using ImageJ 1.0 (FIJI).

For manuscripts utilizing custom algorithms or software that are central to the research but not yet described in published literature, software must be made available to editors/reviewers. We strongly encourage code deposition in a community repository (e.g. GitHub). See the Nature Research guidelines for submitting code & software for further information.

Data

Policy information about availability of data

All manuscripts must include a data availability statement. This statement should provide the following information, where applicable:

- Accession codes, unique identifiers, or web links for publicly available datasets
- A list of figures that have associated raw data
- A description of any restrictions on data availability

The data that support these findings are available from the authors upon request.

Field-specific reporting

Please select the one below that is the best fit for your research. If you are not sure, read the appropriate sections before making your selection.

☒ Life sciences ☐ Behavioural & social sciences ☐ Ecological, evolutionary & environmental sciences

For a reference copy of the document with all sections, see nature.com/documents/nr-reporting-summary-flat.pdf

Life sciences study design

All studies must disclose on these points even when the disclosure is negative.

Sample size	When possible, sample sizes were determined using power analysis. Otherwise, sample sizes were chosen according to previous experiments (Stagkourakis et al. 2018, Falkner et al. 2016, Golden et al. 2016, and Lin et al. 2011)
Data exclusions	Data points were excluded if they were statistically significant outliers according to Grubb's test for outliers. This test was only performed once per data set. In experiments requiring viral infection of a specific brain region, mice were excluded from behavioral analysis if the virus was found to be mis-targeted or not expressed according to pre-determined anatomical criteria. No data was excluded for other reasons.
Replication	When possible, data was collected using biological replicates (e.g. samples run in triplicate for qPCR, multiple brain slices per animal analyzed for in-situ hybridization). All attempts at replication were successful.
Randomization	Animals and samples were assigned randomly to control and experimental groups, except in cases where aggressive behavior was compared between groups. In these cases, aggresison was assessed and groups were counter-balanced for equal levels of aggression before manipulations were performed.
Blinding	While experimenters were not blind to group allocation for data collection, analyses were performed blind to experimental conditions (Behavioral scoring from videos, fiber photometry analysis, quantification of in-situ hybridization results).

Reporting for specific materials, systems and methods

We require information from authors about some types of materials, experimental systems and methods used in many studies. Here, indicate whether each material, system or method listed is relevant to your study. If you are not sure if a list item applies to your research, read the appropriate section before selecting a response.

Materials & experimental systems

n/a	Involved in the study
☐	☒ Antibodies
☐	☒ Eukaryotic cell lines
☒	☐ Palaeontology
☐	☒ Animals and other organisms
☒	☐ Human research participants
☒	☐ Clinical data

Methods

n/a	Involved in the study
☒	☐ ChIP-seq
☒	☐ Flow cytometry
☒	☐ MRI-based neuroimaging

Antibodies

Antibodies used	goat anti-Orexin-A (Santa Cruz Biotechnology, polyclonal, sc-8070; lot: J1818; 1:500); chicken anti-GFP (Aves Labs, monoclonal, GFP-1020; lot: 879484 ;1:1000).
Validation	According to manufacturers, goat polyclonal IgG anti-Orexin-A was validated in mouse and human tissue for immunofluorescence. This antibody has been utilized in previous publications to detect orexin-A in mice using immunofluorescence (Whiddon et al. 2013). According to manufacturers, chicken monoclonal anti-GFP IgY was validated in transgenic mice expressing GFP using immunofluorescence. This antibody has been used in previous publications to detect GFP in mice using immunofluorescence (Daviaud et al. 2018).

Eukaryotic cell lines

Policy information about cell lines

Cell line source(s)	N2A cells were obtained from ATCC (Manassas, VA)
Authentication	The cell lines were not authenticated.
Mycoplasma contamination	Cells were not tested for mycoplasma contamination.

Commonly misidentified lines (See ICLAC register)	No commonly misidentified cell lines were used in this study.

Animals and other organisms

Policy information about studies involving animals; ARRIVE guidelines recommended for reporting animal research

Laboratory animals	CD1: Obtained from Charles River labs (male, 4-6 months of age, cat. CRL22) AD2tm2(cre)/Zjh: Obtained from Jackson Laboratory (3 months of age, cat. 010802). Mice obtained from Jackson Laboratory were crossed with CD1 wild-type mice for one generation to generate GAD2-CRe/CD1 F1 hybrids. Male F1 hybrids 4-6 months of age were used for experiments. Female F1 hybrids were co-housed with F1 males prior to testing. Orexin-Cre-IRES-GFP: Gift from A. Yamanaka (3 months of age, reference: Inutsuka et al. 2014) . Mice obtained from Dr. Yamanaka were crossed with CD1 mice for one generation to generate Orexin-Cre/CD1 hybrids. Male F1 hybrids 4-6 months of age were used for experiments. C57BL6/J: Obtained from Jackson Laboratory (male, 2 months of age, cat. 000664). These mice were used as social targets and not studied here.
Wild animals	This study did not involve wild animals.
Field-collected samples	This study did not include field-collected samples.
Ethics oversight	Mouse experiments were performed in accordance with the National Institutes of Health Guide for Care and Use of Laboratory Animals and the Icahn School of Medicine at Mount Sinai Institutional Animal Care and Use Committee.

Note that full information on the approval of the study protocol must also be provided in the manuscript.

nature neuroscience

SUPPLEMENTARY INFORMATION

https://doi.org/10.1038/s41593-020-0617-7

In the format provided by the authors and unedited.

Orexin signaling in GABAergic lateral habenula neurons modulates aggressive behavior in male mice

Meghan E. Flanigan[1,2], Hossein Aleyasin[1,2], Long Li[1,2], C. Joseph Burnett[1,2], Kenny L. Chan[1,2], Katherine B. LeClair[1,2], Elizabeth K. Lucas[1,2,3], Bridget Matikainen-Ankney[1,2], Romain Durand-de Cuttoli[1,2], Aki Takahashi[1,2,4], Caroline Menard[1,2,5], Madeline L. Pfau[1,2], Sam A. Golden[6], Sylvain Bouchard[1,2], Erin S. Calipari[1,2,7], Eric J. Nestler[1,2], Ralph J. DiLeone[8], Akihiro Yamanaka[9], George W. Huntley[1,2], Roger L. Clem[1,2] and Scott J. Russo[1,2] ✉

[1]Nash Family Department of Neuroscience, Icahn School of Medicine at Mount Sinai, New York, NY, USA. [2]Friedman Brain Institute, Icahn School of Medicine at Mount Sinai, New York, NY, USA. [3]Department of Molecular Biomedical Sciences, North Carolina State University, Raleigh, NC, USA. [4]Laboratory of Behavioral Neuroendocrinology, University of Tsukuba, Tsukuba, Ibaraki, Japan. [5]Department of Psychiatry and Neuroscience, Faculty of Medicine and CERVO Brain Research Center, Université Laval, Ville de Québec, QC, Canada. [6]Department of Biological Structure, University of Washington, Seattle, WA, USA. [7]Department of Pharmacology, Vanderbilt University School of Medicine, Nashville, TN, USA. [8]Department of Psychiatry, Yale University, New Haven, CT, USA. [9]Department of Neuroscience II, Research Institute of Environmental Medicine, Nagoya University, Nagoya, Japan. ✉e-mail: scott.russo@mssm.edu

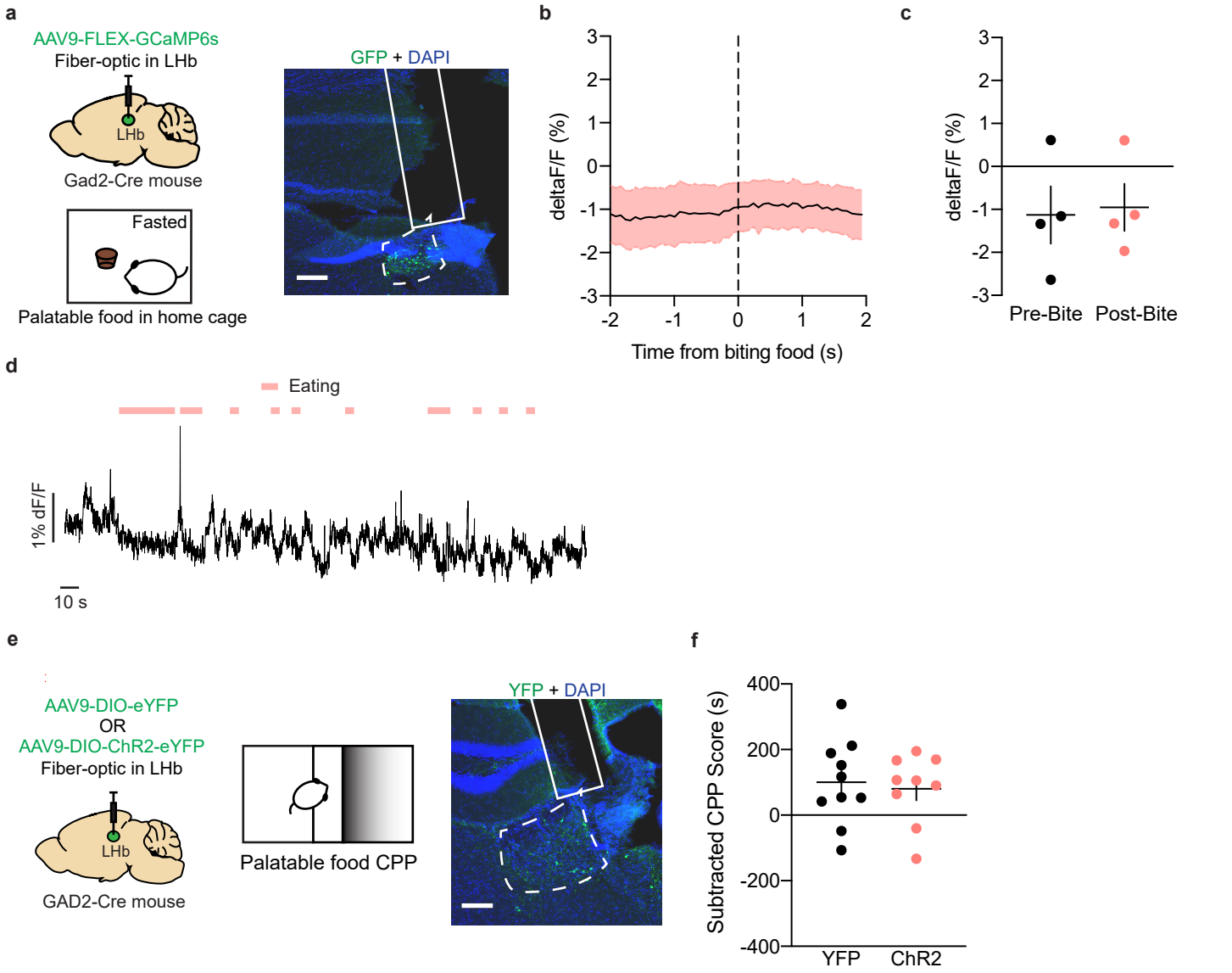

Supplementary Figure 1: LHb GAD2 neurons are not involved in palatable food reward. a, Surgical manipulations and representative viral infection image for LHb GAD2 neuron palatable food reward photometry experiments, scale bar = 400 µm. **b**, Peri-event plot of LHb GAD2 activity 2s before and after biting palatable food in a fasted state in the home cage. Black line denotes mean signal for all animals while pink shading denotes SEM, n=4 biologically independent mice. **c**, Average LHb GAD2 neuron activity was not different before and after the bite (two-tailed paired t-test, n=4 biologically independent mice, t(3)=1.077, p=0.3603). **d**, Representative trace of LHb GAD2 neuron activity during exposure to palatable food in the home cage. **e**, Surgical manipulations and representative viral infection image for LHb GAD2 palatable food CPP optogenetics (ChR2) experiments, scale bar =200 µm. **f**, ChR2-mediated optogenetic stimulation of LHb GAD2 neurons during the palatable food CPP test did not alter the amount of time spent in the palatable food-paired context (two-tailed student's t-test, n=10 biologically independent YFP mice and n=9 biologically independent ChR2 mice, t(17)=0.3572, p=0.7253). All data are expressed as mean + SEM.

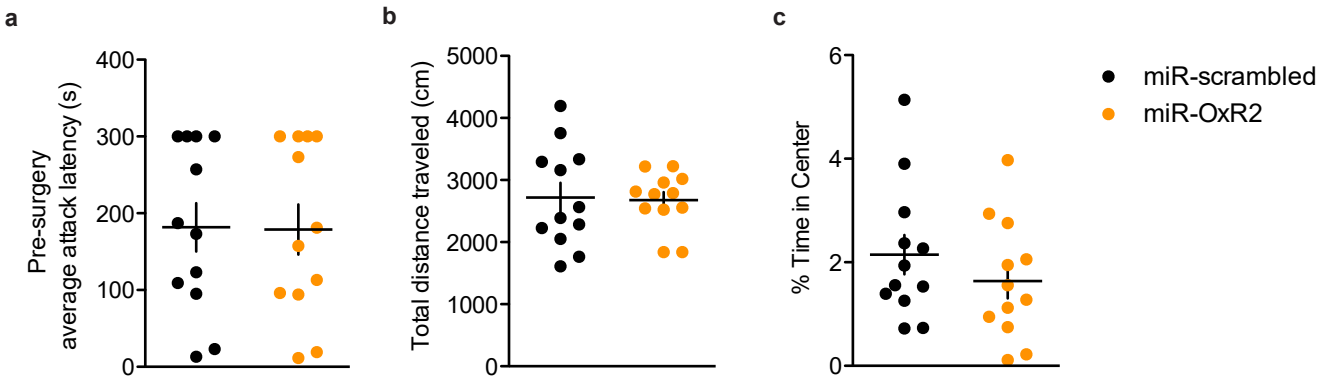

Supplementary Figure 2: **Pre-surgery attack latency, locomotor behavior, and anxiety-related behavior for GAD2-cre mice treated with miR-scrambled or miR-OxR2 viruses. a**, miR-scrambled and miR-OxR2 mice did not display differences in attack latency before surgery (two-tailed student's t-test, n=12 biologically independent mice per group, t(22)=0.0693, p=0.946). **b**, Following surgery, miR-OxR2 mice did not display differences in total distance traveled in the open field compared to miR-scrambled mice (two-tailed student's t-test, n=12 biologically independent mice per group, t(22)=0.1639, p=0.8713). **c**, miR-OxR2 mice did not display any differences in anxiety-related behavior in the open field compared to miR-scrambled mice (two-tailed student's t-test, n=12 biologically independent mice per group, t(22)=1.012, p=0.3224. All data are expressed as mean + SEM.